Alma Mater Studiorum - University of Bologna

School of Engineering and Architecture

Department of Industrial Engineering
Second-cycle Degree in Mechanical Engineering

Master degree thesis

in
Internal Combustion and Hybrid Engines M

Development of a Predictive Thermal Management Function for Plug-in Hybrid Electric Vehicles

Candidate
Alessandro Capancioni

Advisor
Ch.mo Prof. Nicolò Cavina

Co-Advisors
Ing. Michele Caggiano
Ing. Lorenzo Morini
Prof. Davide Moro
Prof. Enrico Corti

Academic Year 2016-2017
Session III

Alma Mater Studiorum - Università di Bologna

Scuola di Ingegneria e Architettura

Dipartimento di Ingegneria Industriale
Corso di Laurea Magistrale in Ingegneria Meccanica

Tesi di laurea

in

Motori a Combustione Interna e Propulsori Ibridi M

Development of a Predictive Thermal Management Function for Plug-in Hybrid Electric Vehicles

Candidato
Alessandro Capancioni

Relatore
Ch.mo Prof. Nicolò Cavina

Correlatori
Ing. Michele Caggiano
Ing. Lorenzo Morini
Prof. Davide Moro
Prof. Enrico Corti

Anno Accademico 2016-2017
Sessione III

Alla mia famiglia,
e a tutti quelli che hanno creduto in me.

Non esiste il brutto tempo,
solo i vestiti sbagliati.

[Proverbio Norvegese]

Abstract

Due to the increasing of individual mobility over the past decades, emissions of noxious pollutant agents such as carbon dioxide and other greenhouse gases have become a non-negligible issue to be deal with. In automotive sector, whereas from a legislative perspective a new driving test procedure has been developed in order to consider effective on-road emissions, the concept of vehicle hybridisation has begun to spread as a possible and challenging solution for CO_2 reduction problem. In particular, electrical hybridisation allows the electrification of several actuators and thus the increasing of the degrees of freedom available for vehicle control strategies. As a result, the on-board energy management can be optimized in order to improve the global efficiency of the vehicle, achieving the goal of fuel consumption reduction. For this purpose, Advanced Driver Assistance Systems (ADAS) can play an important role. They are based on the usage of on-board sensors and enhanced digital map in order to improve driver safety and comfort. Moreover, since navigation systems are increasingly entering the vehicle, the available map data may not only be used for routing purposes, but also to develop advanced in-vehicle features. Thus, ADAS-provided data can support the reconstruction of the electronic horizon which represents a detailed preview of the road ahead by mean of the knowledge of traffic lights time-tables, possible cars accidents and along with others.

The present thesis is focused on the development of a predictive control strategy oriented to battery thermal management for plug-in hybrid electric vehicles (PHEVs). The basic principle of the strategy is to reduce as much as possible battery energy usage related to power request from the respective cooling circuit actuators. At this end, a thermo-hydraulic model of the in-vehicle battery cooling circuit has been developed in AMESim environment. Then, it has been implemented in an already existing Simulink vehicle model, which includes components analytical models

and control strategies. The predictive aspect of the novel strategy is related to the evaluation of battery temperature over the electronic horizon on the base of input signals such as vehicle speed and road slope profile. As a consequence of temperature prediction, the developed strategy is able to establish in an energy-efficient way if cooling power is either required or not. Results highlight the advantages of applying the predictive strategy instead of a rule-based one, which is on-board implemented in each vehicle. It is shown that major energetic benefits, related to the extension of the all-electric range and the reduction of fuel consumption, take place at middle environmental temperatures, at which battery cooling power request can seriously make the difference on its drain rate. Therefore, project goal has been reached and the results can be considered an interesting starting point for further development and enhancing of predictive control strategies.

Abstract in lingua italiana

A causa dell'incremento della mobilità individuale negli ultimi decenni, le emissioni di pericolosi agenti inquinanti quali l'anidride carbonica e altri gas serra sono divenute un problema da affrontare non trascurabile. In ambito automotive, mentre da un punto di vista legislativo una nuova procedura di omologazione di ciclo di guida è stata messa a punto per tenere in considerazione delle reali emissioni su strada, il concetto di ibridazione del veicolo ha iniziato a diffondersi come possibile e interessante soluzione per risolvere il problema legato alla riduzione di CO2. In particolare, l'ibridazione elettrica permette l'elettrificazione di numerosi attuatori e quindi l'incremento dei gradi di libertà disponibili per le strategie di controllo veicolo. Di conseguenza, la gestione dell'energia a bordo può essere ottimizzata per aumentare l'efficienza globale del veicolo, raggiungendo l'obiettivo di ridurre il consumo di combustibile. A tal scopo, sistemi avanzati di aiuto alla guida (ADAS) possono avere un ruolo determinante. Essi sono basati sull'utilizzo di sensori a bordo e mappe digitali avanzate con lo scopo di migliorare la sicurezza e il comfort di guida del conducente. Inoltre, poiché i sistemi di navigazione stanno crescentemente entrando a far parte del veicolo, i dati di navigazione possono essere impiegati non solo per scopi legati al tragitto da compiere, ma anche per sviluppare funzionalità avanzate disponibili in veicolo. Quindi, le informazioni provenienti dai sistemi ADAS possono supportare la ricostruzione di un orizzonte elettronico, il quale rappresenta una anteprima dettagliata del tragitto da percorrere per mezzo della conoscenza della fasatura dei semafori, di eventuali incidenti stradali e altro ancora.

La presente tesi è incentrata sullo sviluppo di una strategia di controllo predittiva orientata alla gestione termica della batteria di veicoli ibridi elettrici plug-in (PHEV). Il concetto di base della strategia è ridurre il più possibile l'utilizzo di energia della batteria relativa alla richiesta di potenza da parte degli attuatori del

relativo circuito di raffreddamento. A questo scopo, un modello termo-idraulico del circuito di raffreddamento della batteria presente in veicolo è stato sviluppato in ambiente AMESim. In seguito, esso è stato implementato in Simulink in modello già esistente del veicolo, il quale include i modelli analitici dei componenti e le strategie di controllo. L'aspetto predittivo della nuova strategia è legato al calcolo della temperatura della batteria all'interno dell'orizzonte elettronico sulla base di segnali di input come i profili di velocità del veicolo e di pendenza della strada. In conseguenza alla predizione della temperatura, la strategia sviluppata è in grado di stabilire in maniera energeticamente efficiente se sia necessario o meno asportare potenza termica. I risultati evidenziano i pregi dell'applicazione della strategia predittiva rispetto a quelli dovuti ad una strategia a regole fisse, la quale è implementata a bordo di ogni veicolo. Si è mostrato che i maggiori vantaggi in termini energetici, legati all'aumento della distanza percorribile in puro elettrico e alla riduzione di consumo di combustibile, si ottengono a medie temperature ambiente, alle quali la richiesta di raffreddamento della batteria può fare la differenza sulla sua velocità di scarica. Quindi, l'obiettivo del progetto è stato raggiunto e i risultati ottenuti possono essere considerati come un interessante punto di partenza per sviluppi e miglioramenti futuri di strategie di controllo predittive.

Acknowledgments

Numerose sono le persone che direttamente o indirettamente hanno contribuito alla realizzazione di questa tesi. Innanzitutto, voglio ringraziare il Prof. Nicolò Cavina per avermi dato la grande possibilità di cimentarmi in questa attività innovativa ed interessante e l'Ing. Michele Caggiano per avermi permesso di realizzarla. Ringrazio anche l'Ing. Lorenzo Morini, l'Ing. Luca Brocchi e l'Ing. Gabriele Caramia per gli indispensabili consigli tecnici ma anche e soprattutto per la professionalità e la disponibilità con cui mi hanno costantemente seguito ed aiutato. Ringrazio, inoltre, i compagni di corso, i coinquilini di Villa Preda e gli amici di una vita che mi hanno supportato e sopportato durante questo lungo percorso di studi. Infine, ringrazio la mia famiglia, in particolar modo mia madre, mio padre e mia sorella, per l'incessante sostegno con cui mi hanno motivato a raggiungere tutti i traguardi più importanti della mia vita. Devo moltissimo a loro, e spero quindi di averli resi fieri e orgogliosi di me.

Perché da soli non si può fare nulla. Grazie.

Contents

List of figures

List of tables

Nomenclature

Acronyms

ADAS	Advanced Driver Assistance System
ADASIS	Advanced Driver Assistance System Interface Specifications
BEV	Battery Electric Vehicle
BMS	Battery Management System
BTM	Battery Thermal Management
BTMS	Battery Thermal Management System
eHS	electronic Horizon Strategy
EM	Electric Motor
ESS	Energy Storage System
EV	Electric Vehicle
GHG	Green-House Gas
GIS	Geographical Information System
HCU	Hybrid Control Unit
HT	High Temperature
HV	Hybrid Vehicle; High-Voltage
HVAC	Heating, Ventilation and Air Conditioning
ICE	Internal Combustion Engine
ISG	Integrated Starter Generator
LIDAR	LIght Detection And Ranging
LT	Low Temperature
MAC	Mobile Air-Conditioning (system)
MiL	Model-in-the-Loop
MPC	Model-Predictive Control

MT	Middle Temperature
NEDC	New European Drive Cycle
ODE	Ordinary Differential Equation
PEMS	Portable Emission Measuring System
PHEV	Plug-in Hybrid Electric Vehicle
PTC	Positive Temperature Coefficient
RADAR	RAdio Detection And Ranging
RBS	Rule-Based Strategy
RDE	Real-Driving Emissions (test)
RMSE	Root-Mean-Square Error
SoC	State of Charge
TXV	Thermal eXpansion Valve
V2C	Vehicle-To-Cloud
V2I	Vehicle-To-Infrastructure
V2P	Vehicle-To-Pedestrian
V2V	Vehicle-To-Vehicle
V2X	Vehicle-To-Everything
WLTC	Worldwide harmonized Light vehicles Test Cycle
WLTP	Worldwide harmonized Light vehicles Test Procedure

Symbols

$b(\cdot)$	control bit of actuators activity [-]
Δ	change
$\Delta_{\%}$	percentage change
$C(\cdot)$	electric capacity [Ah]
$u(\cdot)$	control (output) signal
$\eta(\cdot)$	efficiency [-]
$F(\cdot)$	force [N]
g	gravitational acceleration [m/s^2]
$i(\cdot)$	input signal
J	moment of inertia [kg·m^2]
m, M	mass [kg]

N	number [-]
$P(\cdot)$	power [W]
γ	gear ratio [-]
r	radius [m]
$R(\cdot)$	resistance [Ω]
$\alpha(\cdot)$	angle of slope [rad]
$\alpha_{\%}(\cdot)$	percentage road slope [%]
$\xi(\cdot)$	state of charge (of the high voltage battery) [-]
$x(\cdot)$	state variable
$\omega(\cdot)$	revolution speed [rad/s]
c_p	specific heat capacity at constant pressure [J/(kg·K)]
$n(\cdot)$	revolution speed [rpm]
$v(\cdot)$	longitudinal speed [km/h]
$\tau(\cdot)$, $T(\cdot)$	temperature [℃]
t	time [s]
$T(\cdot)$	torque [Nm]
$V(\cdot)$	voltage [V]

Subscripts

$_a$	aerodynamic
$_{\text{amb}}$	ambient
$_{aux}$	auxiliaries
$_b$	high voltage battery
$_{\text{cpr}}$	compressor
$_{\text{c}}$	city
$_{\text{c}}$	high-voltage battery cell
$_{\text{cab}}$	vehicle cabin
$_{cd}$	coast-down
$_{ch}$	charging
$_{dc}$	DCDC
$_{dh}$	discharging
$_{\text{ice}}$	internal combustion engine

el	electric, electrical
eq	equivalent
f	frontal
g	gradient
j	inertial (force)
0	initial value
in	input; event start
los	loss, losses
m	(electric) motor
mec	mechanical
mot	motoring (force, torque)
oc	open circuit
out	output; event end
pmp	pump
r	rear; rolling
res	resistant (force, torque)
p	parallel-connected
s	series-connected
tr	transmission
t	traction
v	vehicle
w	wheel
wall	vehicle wall

Chapter 1

Introduction

1.1 Overview

In the last century the spreading of industrialization has led to an incessantly growing emission of carbon dioxide (CO_2) and other greenhouse gas (GHG) which represents one of the most demanding challenges of present times, global warming. This issues is even related to automotive sector, in which individual mobility has been increasing over the past decades.

This issue, in conjunction with the large and growing proved discrepancies between laboratory (NEDC) and on-road emissions, especially for nitrogen oxide (NO_x) emissions from diesel cars, has led to the development of a real-driving emissions (RDE) test procedure by the European Commission. Such a kind of test does not replace the WLTP laboratory test, but complements it. In the RDE cycle, a car is driven on public roads and over a wide range of different conditions which are designed to be representative of driving conditions normally encountered on European roads [1]. On-board emissions measuring is performed by means of Portable Emission Measuring Systems (PEMS) that provide a complete real-time monitoring of the key pollutants emitted by the vehicle.

Moreover, in addiction to European legislations, a possible an interesting technical solution in order to overtake the global noxious emissions challenge can be represented by vehicle powertrain hybridization. In hybrid vehicles (HV), two or more

power sources are employed in order to satisfy driver torque demand. As a consequence, additional degrees of freedom concerning on-board energy management are introduced, which implies the development of more complex control strategies. Despite this disadvantage, several ways now can be pursued in order to optimize energy use, with particular attention to fuel consumption minimization. Moreover, the adoption of an hybrid architecture allows energy recuperation, which can be achieved by regenerative breaking, for example. Even though several auxiliary energy sources have been taken into account for hybridization, the most widely-spread hybrid vehicles are hybrid electric vehicles (HEV), which use a high-voltage battery as an additional energy storage system. If the electric energy used for propelling can be derived from renewable energy sources, this vehicle technology is a promising way to reduce global warming. However, the biggest challenge for this kind of vehicles is still the storage capacity of electric energy.

Concerning HEVs, three categories based on powertrain layout and thus energy flow can be defined, which are

- *series* topology
  it is similar to a pure electric drivetrain with the addition of the engine as an auxiliary power unit;

- *parallel* topology
  both the engine and the electric motor(s) can directly propel the vehicle;

- *power-split* topology
  both series and parallel working modes can be applied.

With regard to HEVs parallel topology, several architectures based on electric machines position within the driveline are possible. As shown in Fig. 1.1, they are as follow

- P0
  the motor is coupled to the engine by mean of a belt. In this case, the electric machine is called BSG (Belt-driven Starter Generator);

- P1
  the motor/generator is directly mounted on the crankshaft upstream of the clutch. Here, the motor is an ISG (integrated Starter Generator)

- P2
  the motor is decoupled from the engine by a clutch and pure electric drive is now feasible;

- P3
  the motor is mounted on the secondary shaft of the gearbox;

- P4
  the motor is directly mounted on the front or rear axle.

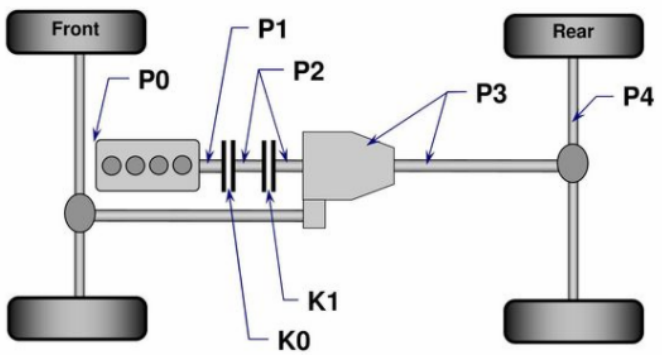

Figure 1.1: Parallel hybrid architectures.

In the present work, the vehicle in exam is a P1-P4 plug-in hybrid electric vehicle (PHEV), which is a hybrid electric vehicle that can be recharged directly from the grid or by the in-vehicle generator as well as the engine. Therefore, an ISG is present an two electric machines mounted on the front axle are available to supply wheels torque demand. Compared to the other alternatives, a relevant benefit related to P4 architecture is the higher efficiency of energy recuperation because of motors are directly coupled to the wheels, avoiding power losses in the transmission during regenerative brakings. This means the only efficiency to be considered is the electric machines one.

1.1.1 ADAS and electronic horizon

Advancements in wireless communication technologies, sensor fusion, imaging technologies, Big Data, and analytics have created opportunities for automotive

manufacturers to discover a wide range of solutions for multiple applications. Miniaturization of electronic components, advancements in navigation, and adoption of smart devices is expected to fuel advancements in the vehicle-to-everything (V2X) communications industry.

V2X technologies include:

- Vehicle-to-Vehicle (V2V)
- Vehicle-to-Infrastructure (V2I)
- Vehicle-to-Cloud (V2C)
- Vehicle-to-Pedestrian (V2P)

and it is expected to show high growth potential for the development of future connected cars that will be able to interact with the environment around.

With regard to the actual self-driving car revolution, the concept of *autonomy levels* has been proposed by the international Society of Automotive Engineers (SAE) in [2]. In Fig. 1.2 a schematic representation of these levels is shown, which span from no automation (Level 0) to full automation (Level 5).

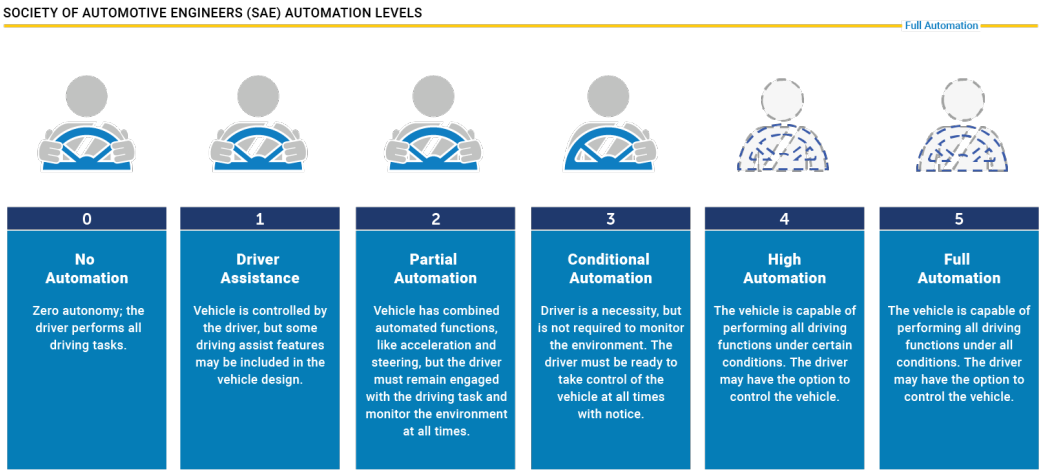

Figure 1.2: SAE automation levels for self-driving vehicles [2].

To this aim, on-board vehicle sensors play a vital role on driving automation, providing the spreading concept of data fusion in order to improve navigation data

availability as well as reconstruct an electronic horizon of the upcoming events. As shown in Fig. 1.3, these sensors include

- LIDAR (LIght Detection And Ranging)
  surveying method that measures distance to a target by illuminating that target with a pulsed laser light;
- RADAR (RAdio Detection And Ranging)
  object-detection system that uses radio waves to determine the range, angle, or velocity of road objects;
- camera
  a video sensor used to analyse the environment outside and inside the vehicle.

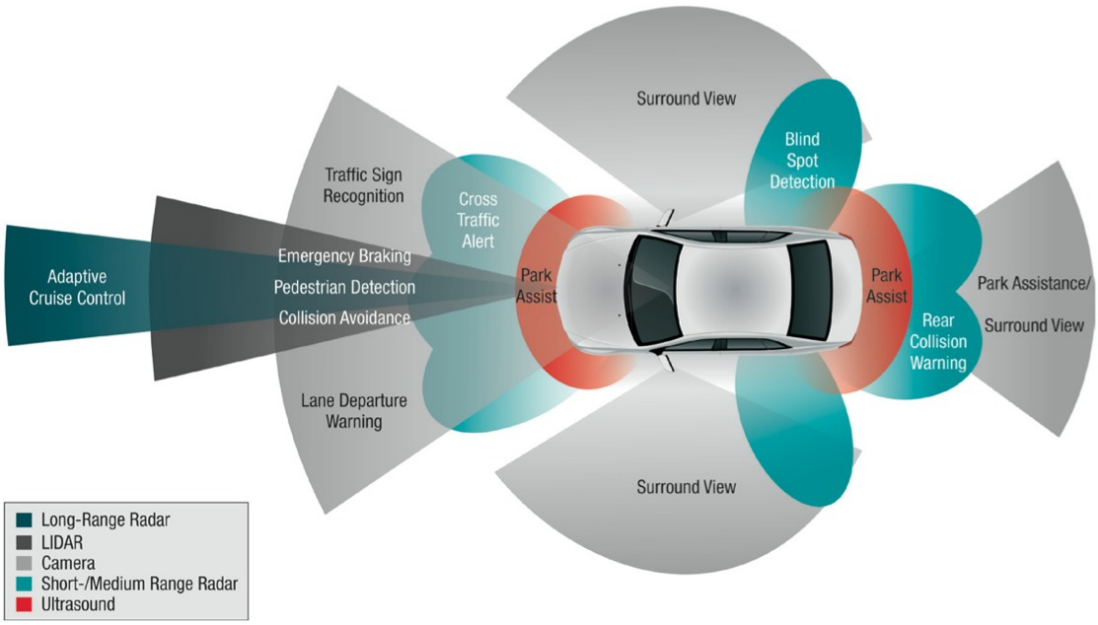

Figure 1.3: On-board vehicle sensors.

Since navigation systems are increasingly entering the automotive sector, the available map data may not only be used for routing purposes but also to enable advanced in-vehicle applications. The area of potential features reaches from headlight control up to active safety applications (ADAS1). With the ongoing development of navigation based ADAS features the interface to access the so-called ADAS Horizon

is of rising importance. At this end, Advanced Driver Assistant Systems Interface Specifications (ADASIS) is an industrial platform where map provider and automotive developers work together to standardize the map data. The method of how a vehicle's control unit could be provided with the navigation data is specified as well in the ADASIS protocol [3].

The map data thereby dispose of a much greater range and complete the information provided by common radar, video and ultrasound sensors. Therefore, eHorizon is focused on integrating topographical and digital map data with sensors data for predictive control of vehicle systems. The electronic horizon is based on the concept of *transceiver-receiver* dualism. The first one corresponds to the horizon provider and the receiver is called horizon reconstructor, which plays the role of data analyser. They are strictly connected and able to communicate due to the ADAS standardized protocol. As remarked in [3], in-vehicle advanced features can be pursued due to enhanced map attributes, such as speed limits, road inclination, stop points and more over. Predicted events, such as the uphill incline after the next corner, and in the future even dynamic events, such as accidents or traffic jams, are exploited at an early stage in order to optimize the vehicle's response.

From this perspective, the objective of this work is the development of a predictive control strategy based on navigation data in order to consume, for the thermal management, as less electrical energy as possible and consequently decreasing the fuel consumption and NO_x emissions.

Chapter 2

State of art of Thermal Management in PHEVs

2.1 Cooling and heating systems overview

As the major part of the current plug-in HEVs, the cooling system presents a complex architecture due the high number of components to be cooled down. This is all because the high level of electrification of such a kind of vehicles, which introduces the problem of heat power losses due to the presence of current flows. In HEVs, and especially in BEVs, cooling systems have to deal with electrical devices heating, both for a matter of power supply (as in the case of the motors and the traction battery, which efficiency is strictly influenced by their operating temperatures) and state of charge depleting. The latter aspect is indeed taken into account for developing a predictive thermal management control function in order to minimize the power demand of certain cooling circuits actuator, especially the high-voltage compressor which has a consistent impact on battery energy consumption, as later explained.

The latter component is employed in air-conditioning (AC) and battery cooling circuits to perform a *vapour compression refrigeration cycle* which operates a thermal energy removal from a low-temperature ambient to an high-temperature one. The schematic of a single-stage vapour compression cycle is represented in Fig. 2.1 and the components of the circuit are showed in Tab. 2.1.

The operating fluid, called refrigerant, must have certain physical properties such

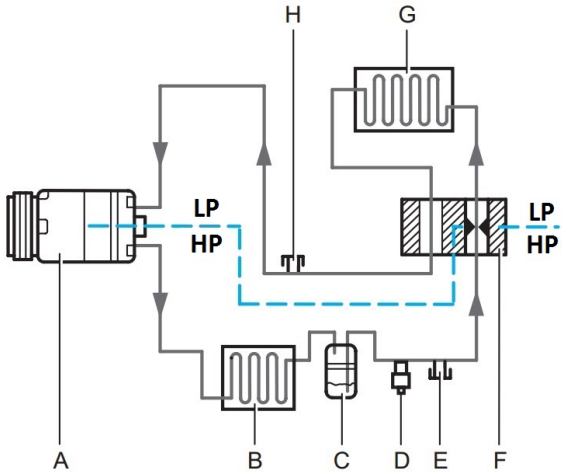

Figure 2.1: Schematic of a single-stage vapour compression cycle-based circuit.

Table 2.1: Components of a single-stage vapour compression cycle-based circuit.

Index	Description
A	Electric compressor with magnetic clutch
B	Condenser
C	Accumulator with drier
D	High-pressure switch
E	High-pressure service connection
F	Expansion device
G	Heat exchanger
H	Low-pressure service connection
HP	High-pressure side
LP	Low-pressure side

as low boiling point at ambient pressure in order to provide a better heat absorption at evaporation side, and environmentally-friendly suitable, thus depletion of the ozone layer in the earth's atmosphere. For these reasons, R134a (a fluorocarbon, FC) refrigerant is used, since R12 (a chlorofluorocarbon, CFC) was banned due to its negative environment-related impact. Moreover, in recent times R1234yf (a synthetic HFO refrigerant) has been developed as a successor to R134a for automotive air-conditioning applications. This innovative solution, which has similar cooling capacity and energy efficiency to R134a, is proposed in order to overcome

the greenhouse gas emissions challenge and thus meet European and world environmental standards. Nevertheless, R1234yf is not only more complex and expensive to produce, but also and in particular is mildly-flammable gas. Therefore, for safety and cost reasons, this alternative refrigerant is not yet widely employed in mobile air-conditioning (MAC) systems.

Cabin cooling is obtained by means of the aforementioned circuit, in which the in-coming air from the external environment is cooled down in the *evaporator*, a vapour-liquid heat exchanger, by the refrigerant. A thermal expansion valve (TXV) controls the refrigerant mass flow rate through the evaporator. This circuit is called *air-conditioning circuit*.

Cabin heating can be whereas obtained in several ways. In general, for conventional and hybrid vehicles, the huge amount of engine thermal power losses is used to heat up the cabin. A specific valve (heater valve) of the engine cooling circuit taps a certain engine coolant flow through an air-liquid heat exchanger (heater core), positioned under the dashboard. A fan draws the environmental air from the outside which gets heated flowing through the heater core.

The aforementioned cabin heating and cooling circuits are depicted in Fig. 2.2.

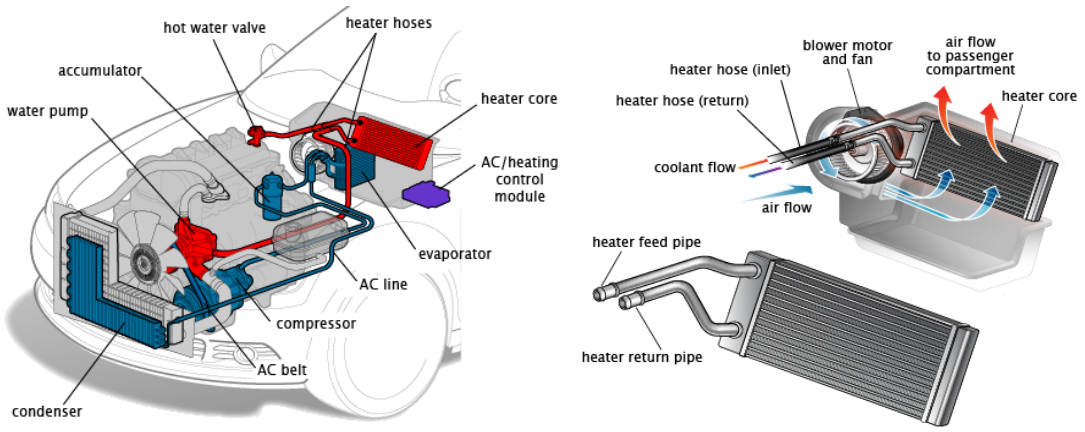

(a) In-vehcile architecture. **(b)** Particular: heater core.

Figure 2.2: Cabin cooling (AC) and heating circuits.

Another technical solution is based on *resistive heating*. Due to the absence of an internal combustion engine, this approach is adopted in EVs and can be found even in PHEVS in conjunction with the classic heating circuit in order to accelerate

cabin heating. For this purpose, positive temperature coefficient (PTC) thermistors are starting to be widely used in automotive applications. Over the majority of its operating temperature range, PTC thermistors exhibit a slight negative temperature coefficient, similar to most of semiconductors. However, as the temperature approaches a certain value, known as the switch temperature, the resistance begins to rise very rapidly. Thus, the current flow through the component decreases and the same do thermal power losses and component temperature. This produces a self-regulating effect.

Despite the benefits of PTC heaters use, including no excess temperature protection required, fast thermal response, compact design and large temperature operating range (from 50℃ up to 320℃) [4], resistive heating implies high electric power consumption, especially in winter scenarios when higher heating system performances are required, leading to an unavoidable pure electric drive range reduction. This represents a serious issues to deal with due to the limited battery energy storage of present vehicles, in particular for EVs in which the high-voltage battery is the only power and traction source. That is why recently *heat pump systems* are being developed and are increasingly spreading as an innovative solution to contain battery energy consumption.

A heat pump system is typically a vapour-compression refrigeration device that includes a reversing valve and optimized heat exchangers so that the direction of heat flow can be reversed. This valve switches the direction of refrigerant through the cycle and therefore the heat pump may either supply or absorb heating power from the cabin. Several technology configurations are possible, which may comprehends the use of PTC heater [5], too.

Moreover, widely popular approaches focused on efficiency-improving targets include different refrigerants, novel components and innovative system structures which actually represents an interesting matter of research.

2.2 In-vehicle cooling system architecture

In order to clarify the structure of the vehicle cooling system, a classification based on the nominal temperature values reached by each component can be made. Thus, three temperature level-based cooling subsystems can be individuated, and

they are the following

1. *Low Temperature (LT)* cooling subsystem
2. *Middle Temperature (MT)* cooling subsystem
3. *High Temperature (HT)* cooling subsystem

With regard to the previous classification, the cooling circuits that have been considered during the present work are listed in Tab. 2.2.

Table 2.2: List of the in-vehicle cooling circuits.

Subsystem	**Circuit(s)**
Low Temperature	Battery-AC integrated circuit
Middle Temperature	Front-axle cooling circuit ISG cooling circuit
High Temperature	Engine cooling circuit

The battery-AC integrated cooling circuit (Fig. 2.3) consists of the following

- battery cooling circuit
  the coolant absorbs heat power from the HV battery flowing through cooling plates and it is then cooled down by the refrigerant in gaseous state by means of a *chiller*, a vapour-liquid heat exchanger. A thermal expansion valve (TXV) controls the refrigerant mass flow rate through the chiller;
- air-conditioning circuit
  the in-coming air from the external environment is cooled down in the *evaporator*, a vapour-liquid heat exchanger, by the refrigerant. A TXV with the same purpose is present, as well.

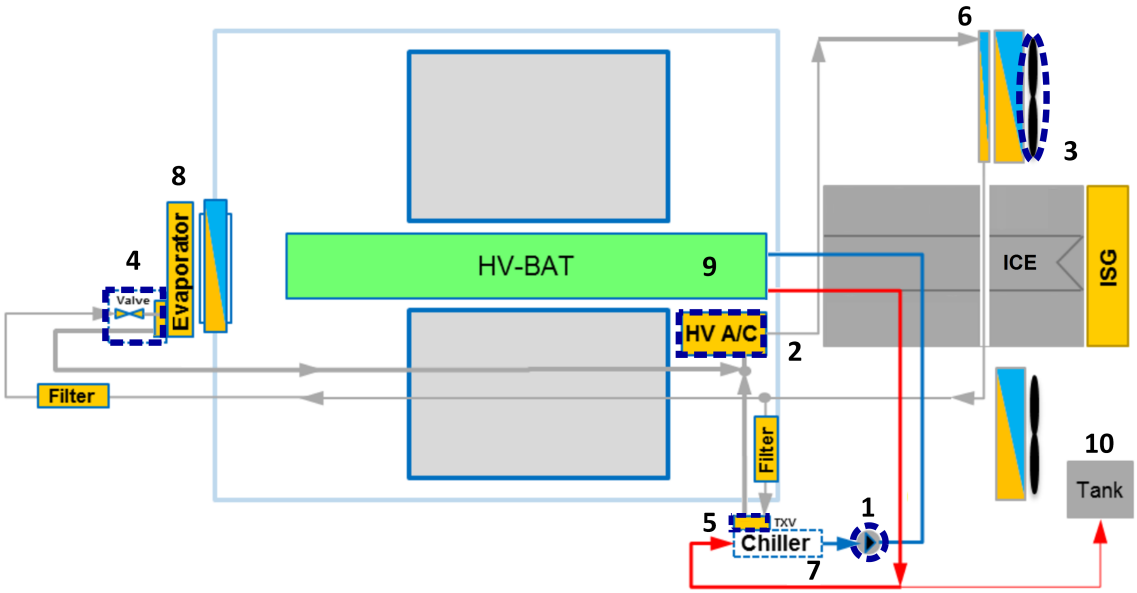

Figure 2.3: Battery-AC integrated circuit layout.

Table 2.3: Actuators and components of the battery-AC integrated circuit.

Type	No.	Name
Actuators	1	Electric pump
	2	High-voltage compressor
	3	Fan
	4	TXV (cabin loop)
	5	TXV (battery loop)
Components	6	Condenser
	7	Chiller
	8	Evaporator
	9	High-voltage battery
	10	Expansion tank

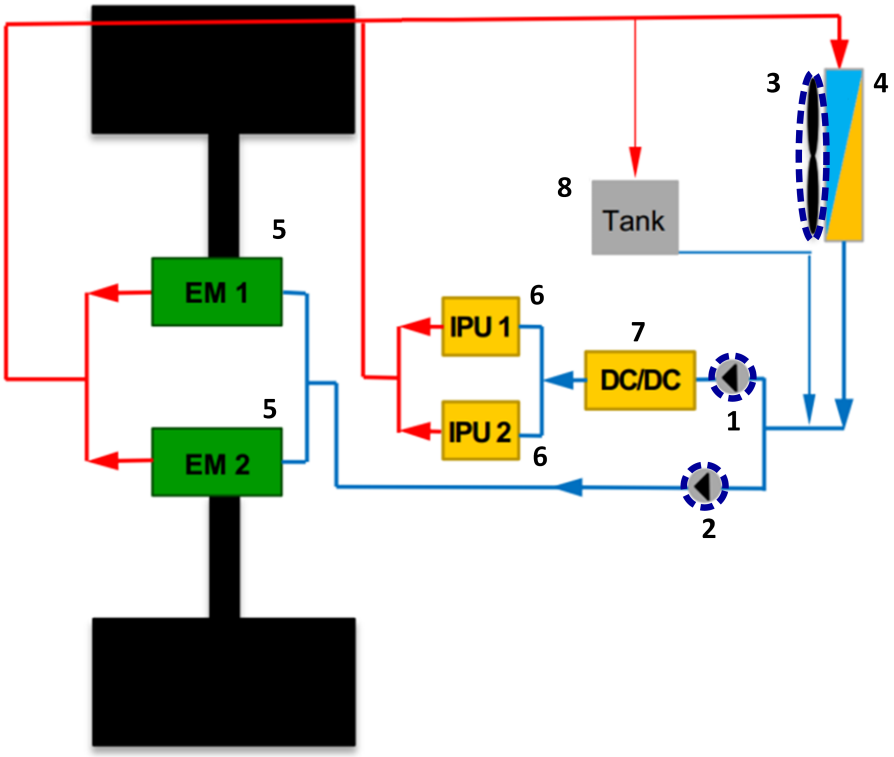

Figure 2.4: Front-axle cooling circuit layout.

Table 2.4: Actuators and components of the front-axle cooling circuit.

Type	No.	Name
Actuators	1	Electric pump (inverters loop)
	2	Electric pump (motors loop)
	3	Fan
Components	4	Radiator
	5	Motors (P4)
	6	Inverters
	7	DCDC
	8	Expansion tank

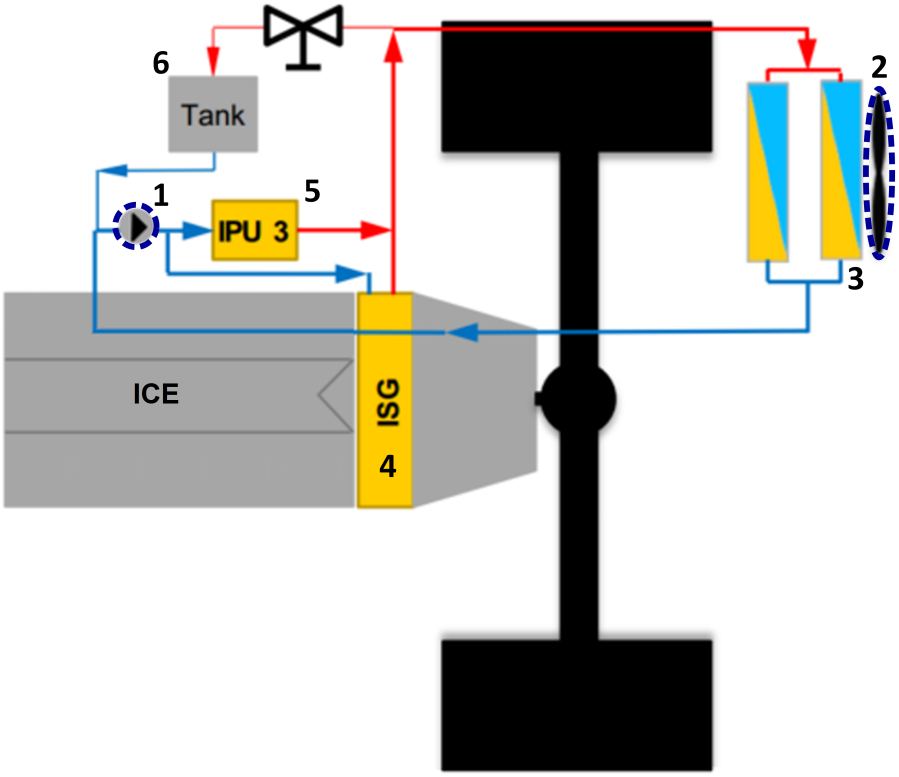

Figure 2.5: ISG cooling circuit layout.

Table 2.5: Actuators and components of the ISG cooling circuit.

Type	No.	Name
Actuators	1	Electric pump
	2	Fan
Components	3	Radiator
	4	ISG (P1)
	5	Inverter
	6	Expansion tank

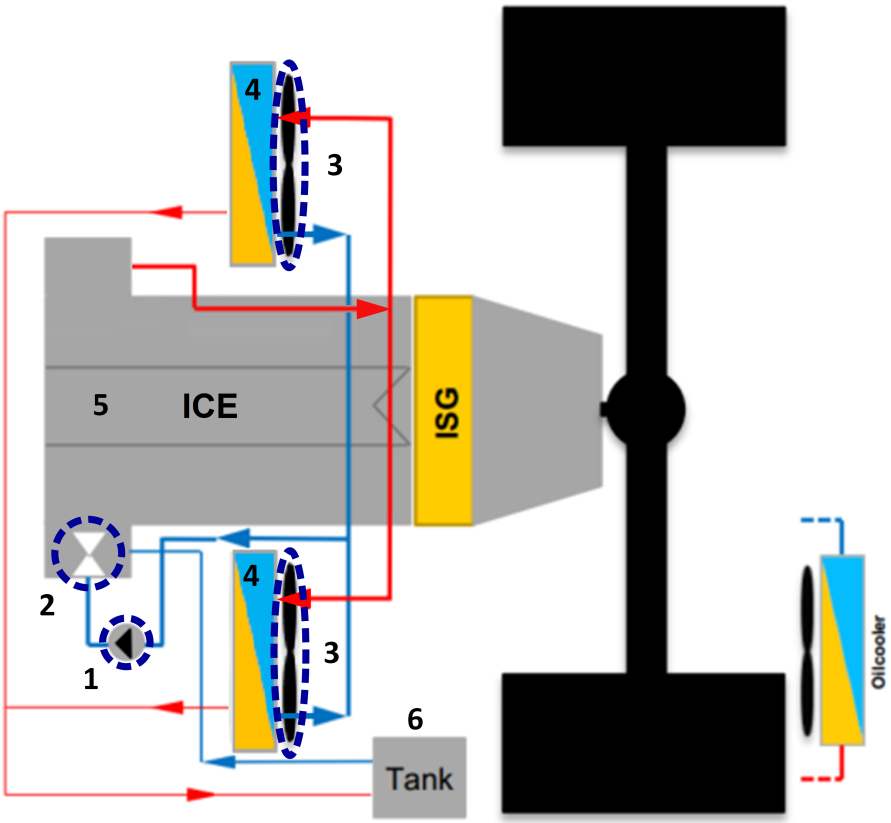

Figure 2.6: Engine cooling circuit layout.

Table 2.6: Actuators and components of the engine cooling circuit.

Type	No.	Name
Actuators	1	Electric pump
	2	Thermostat
	3	Fans
Components	4	Radiators
	5	Engine
	6	Expansion tank

2.3 Thermal management control strategies

The electrical battery pack in HEVs and BEVs must deal with important thermal issues which can seriously compromise reliability, safety and ageing of the involved components [6]. Consequently, an advanced battery control is needed. For this reason, battery management systems (BMS) constantly estimate the state of charge, equalize the charge and thermally manage the cells in order to enhance the safety, cycle-life and performance of the component. Even though the components and the layout of the battery cooling circuit may vary from vehicle to vehicle, their purposes are usually the same, which is creating an efficient and robust system that is not affected by internal and ambient temperature variations.

In particular, battery thermal management system (BTMS) plays a vital role on battery ageing and performances due to the dependence of its efficiency and power supply to the operating temperature, as shown in Fig. 2.7. Thus, its temperature needs to be constantly monitored in order to avoid potentially dangerous conditions as well as allow the component to operate in the most energy-efficient way. Consequently, it is clear that battery temperature must be contained and limited in a well-defined range ($T_b \in [5,45]$°C), which represents an important thermal constrains to be respected by battery thermal management control strategies. Moreover, in order to avoid battery de-rating due too relevant thermal stresses, the upper limit value of the previous range might be reduced to 40°C [7].

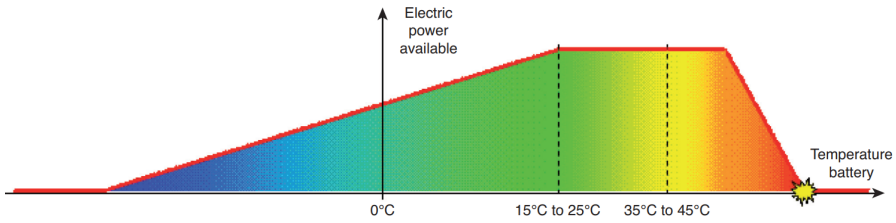

Figure 2.7: Battery power supply as a function of its temperature [8].

Heat is generated and released from the cell during both grid charge and discharge, as well. If the heat generated in the cell/pack is not removed efficiently, then it is stored, raising the temperature of the cell and the total battery pack [9]. An interesting predictive thermal strategy has been proposed and analysed in [8]. The study is focused on the possibility to attain a certain cooling power reduction by

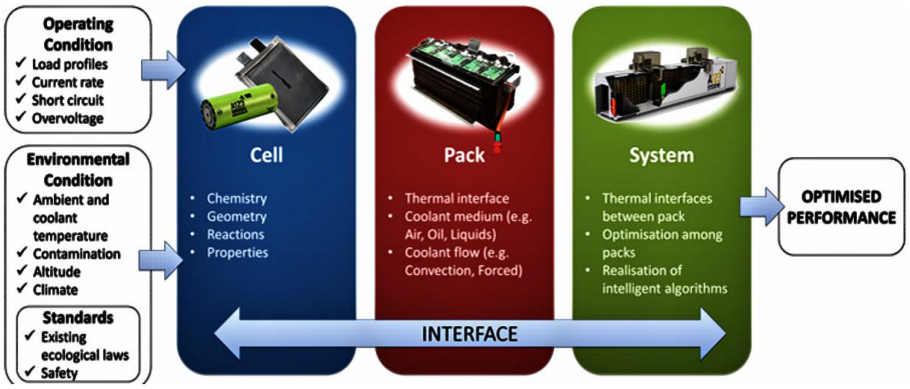

Figure 2.8: Battery thermal managament system (BTMS) architecture [9].

means of *plugged-in battery thermal pre-conditioning*. Results obtained by applying a standard thermal management control strategy and the predictive one are compared in Fig. 2.9. As shown in Fig. 2.9b, during grid charging active pre-conditioning is realised by cooling down the battery to 15℃ and thus no cooling power has to be supplied during the last driving cycles because of battery temperatures doesn't reach the upper threshold set for actuators activation. As a result, this energy-efficient strategy allows a 133 kJ economy inside the battery on the second driving phase of the sequence, with a consequent driving range extension of about 200–300 m, which corresponds to around 2–3% of the whole travelled distance.

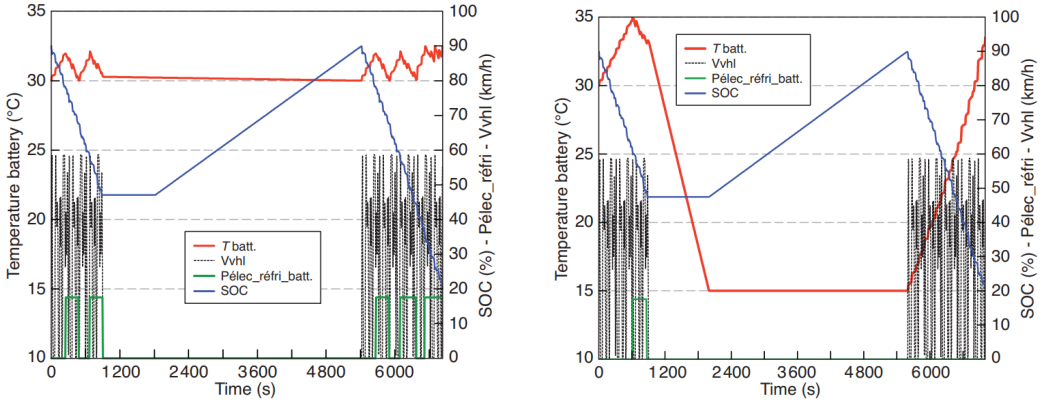

(a) No pre-conditioning. **(b)** Pre-conditioning.

Figure 2.9: Comparison between a standard battery control strategy and plugged-in battery thermal pre-conditioning [8].

Such a kind of thermal management strategy can be employed in vehicles applications by means of the previous described ADAS system, which can provides several navigation data for electronic horizon reconstruction. In other words, the plugged-in battery thermal pre-conditioning can be actuated in the case of the driver is able to set the route destination of the next trip with a certain advance. A typical common situation is represented by a well-known trip which is performed every day to get to the workplace. In this case, the benefit of a predictive strategy is reached once the user set up the journey the night before going to work or when an on-board machine learning-base adaptive system is able to recognize a well-known trip which is recursively performed.

Several ways to employ route information for energy-efficiency targets are under research. One of these is represented by the use of a *Model-Predictive Control* (MPC) strategy in which a process model of the investigated system is developed in order to fully describe the associated thermal dynamics. Such an accurate model is needed to calculate the predicted control output at future instant as a function of several input signals [10]. Thus, the control law can be obtained by optimizing an objective function.

In [11] a control-oriented non-linear model is first developed for the system and a Non-linear Model Predictive Control (NMPC) scheme is formulated to make it possible to use the knowledge of the predicted future drive cycle and the battery thermal system model for an efficient battery thermal management.

An interesting study has been conducted in [12] with the aim of developing an MPC design as an alternative solution for thermal management cabin heating for HEVs. The state variables of the model are the heater core power, the PTC heater power and the incremental engine power request, which are manipulated in order to achieve the best compromise between the following targets: total heat power supplying, fuel consumption minimization and battery SoC preserving within a certain range. The innovative aspect of this research can be individuated in the challenging possibility of the cabin thermal management to influence the vehicle energy management by setting the torque split factor so as to distributing the workload between the heater core and an the PTC heater in an optimal way, i.e. minimizing fuel consumption.

Chapter 3

Control-oriented modelling

The modelling of the previously described heating and cooling circuits is explained as follows.

At first, an overview on the AMESim modelling environment is presented. Then, the physical models used for strategies development and simulations are briefly described, with particular attention to the battery cooling circuit model and its validation.

An analytical HVAC model for cabin energy consumption evaluation has been developed, as well.

Finally, the implementation of the aforementioned models in Simulink control and simulation environment is described, paying attention to the Model-In-the-Loop architecture and the AMESim-Simulink co-simulation mode.

3.1 *LMS Amesim* environment

LMS Imagine.Lab Amesim is a commercial simulation software for the modelling and analysis of multi-domain engineering systems. Its name stands for *Advanced Modeling Environment for performing SIMulations of engineering systems.*

The software package is a suite of tools used to model, analyse and predict the performance of a system and offers plant modelling capabilities to connect to controls design, helping user assess and validate control strategies. Models are described using non-linear time-dependent analytical equations that represent the system's

hydraulic, pneumatic, thermal, electric or mechanical behaviour.

In order to create a simulation model for a certain system, a set of libraries is used. They contain pre-defined *physics components* (for each different domain) which are represented by icons. These have to be connected to each other and for this purpose an icon has several ports, corresponding to inputs and/or outputs. *Causality* is enforced by linking the inputs of an icon to the outputs of another one (and vice versa).

3.1.1 Architecture

Software architecture is depicted in in Fig. 3.1

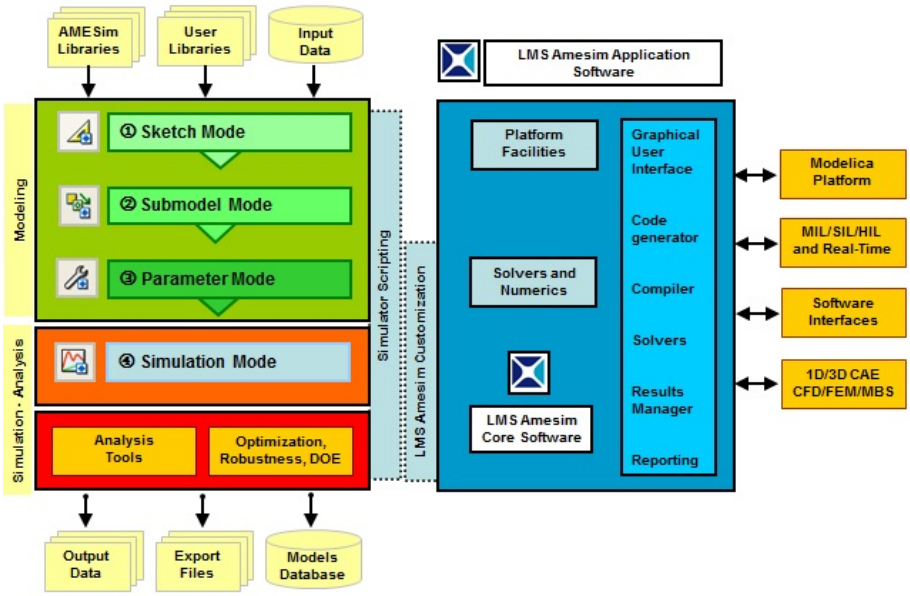

Figure 3.1: LMS Amesim architecture.

This software offers powerful platform features so that any user can easily create an LMS Amesim model from the standard libraries or from user-defined ones, and run it to get analysis results.

Platform facilities ensure the easy use of the models and allow the integration of

the software in the design process. These facilities includes graphical user-friendly interface, *Analysis Tools* (table editor, plots, 3D animation, linear analysis – eigenvalues, modal shapes, transfer functions, root locus), *Simulator Scripting* (using MATLAB, Scilab, Python, Visual Basic), *MIL/SIL/HIL and Real-Time* (co-simulations with Simulink, Labview), *1D/3D CAE* (CFD software co-simulation, FEA import of reduced modal basis with pre-defined frontier nodes, MBS software co-simulation and import/export).

3.1.2 Working modes

In order to built up a complete working model, the following sequential steps must be followed:

1. *Sketch mode*
   Initially, a schematic of the system must be built choosing icons from libraries. Available libraries set is shown in Fig. 3.2. Each library consists of one or more. A category is a collection of special component icons and mathematical models of these components (referred to as *component submodels*). All the ports of the components must be connected.

Figure 3.2: Libraries set in LMS Amesim version v1501.

2. *Submodel mode*
   Every component in the system must be associated with a mathematical

model. This is a collection of mathematical equations and their implementation as a piece of computer code. The particular mathematical mode used to describe a particular component behaviour is called *submodel* (the term *model* is reserved for the mathematical model of the entire system). Assigning submodels must be performed for all the components;

3. *Parametric mode*
   Parameters must be set for each submodel. User has to specify their values. They can be real, integer, text type parameters and many more and can concern geometrical design, working mode of the component, physical data, etc;

4. *Simulation mode*
   The software performs various checks and creates an executable for the system. The *System Compilation* window appears, showing technical information about the equations it must solve to perform a simulation and the number of involved state variables. Moreover, before running the simulation, run parameters can be set (start and final time, single-run/batch simulation, standard/fixed-step integrator, etc.).

3.2 Battery cooling circuit thermo-hydraulic model

All the cooling circuits described in § 2.2 were already modelled, calibrated and validated in AMESim environment during a previous activity [13]. Only the high-voltage battery cooling circuit have been modified and further developed in order to make it adaptable for a control-oriented strategy.

Development

The latter model can be implemented in an integrated system considering the HVAC system loop too, as happens in practice for in-vehicle design solutions. Nevertheless, the significant effort related to the physical development of such a complex system is not hereby justified by the main objective of the present thesis activity, which is the development of a predictive thermal management control function focused on battery thermal behaviour. Anyway, an attempt was made in [13] to model

the integrated system without considering the air-conditioning circuit. For the same aforementioned reasons, it was only developed and not validated. Such a physical model has been taken into account as an important starting point for the development of a control-oriented system. In addiction, an energy-based cabin model has been developed independently from the battery cooling circuit, as explained in detail in § 3.3. In view of this, for *battery cooling circuit model* is hereafter intended the model including the chiller and the condenser loop.

In the developed cooling circuit, the high-voltage compressor, the pump and the fan can be directly controlled with targeted strategies, described in Ch. 4. Only the thermal expansion valve (TXV) is mechanically controlled due to the lack of experimental data. This means that the valve rod lift is not evaluated by a control unit, but by means of valve characteristic maps with the value of the measured temperature and pressure of the refrigerant at chiller outlet as input.

Different libraries have been used for model development, in particular the *Air Conditioning* library for the whole condenser loop and the *Thermal* and the *Mechanical* ones for the chiller loop. In the latter case, a *thermal mass* component has been taken into account for battery thermal dynamics modelling. For the sake of

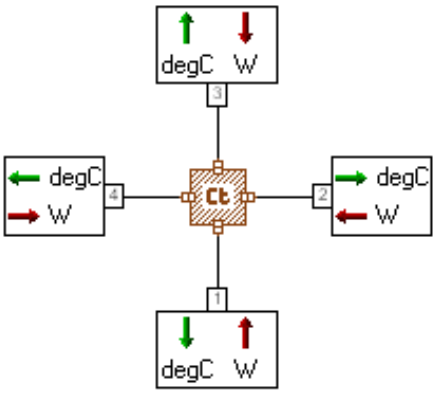

Figure 3.3: Thermal mass component in AMESim environment.

simplicity, an only thermal mass has been used. This component allows to computes the temperature dynamics of a solid mass with respect to incoming heat fluxes [14], which are represented in this case by the thermal power losses and the cooling power supplied by the coolant. The temperature of the thermal mass is the same output

at each port and is evaluated from the energy balance as

$$\frac{dT}{dt} = \frac{1}{m \cdot c_p(T)} \sum_{i=1}^{4} dh_i \tag{3.1}$$

where dh_i is the input heat flux at the i-th port, m is the mass of the component, c_p is the specific heat of the material, expressed as a second-order polynomial in function of the temperature of the component.

It must be clarified that temperature distribution within the battery is not homogeneous; it slightly varies from cell to cell. Because of in the interests of safety the maximum battery temperature is to be taken into account by the BMS, this parameter is here evaluated by supposing that it is 3°C constantly higher than the average temperature, which is the only temperature evaluated by the thermal mass used.

Calibration

For a matter of simplicity, battery cooling circuit model has been calibrated in Simulink environment with the modalities explained in § 3.4.

Battery specific heat capacity has been chosen as the only parameter to be calibrated because of in the previous version of the model it was set on the base of values proposed in literature. Thus, a further calibration step was needed, even considering the several changes made to the physical model.

The calibration process is structured as follows:

- according to the previous value, a plausible range of variation is chosen for the parameter to be calibrated
- several values within the aforementioned domain are considered and a simulation is performed for each of them
- the optimal value is the one which minimizes a certain accuracy indicator

In this case, the normalised root-mean-square error (NRMSE) is considered as estimator of the difference between the experimental and the simulated battery temperature. It can be expressed as follows

$$NRMSE = \frac{RMSE}{\overline{T_{\mathrm{b}}^{e}}} \tag{3.2}$$

where $\overline{T_{\mathrm{b}}^{e}}$ is the mean value of battery experimental temperature and

$$RMSE = \sqrt{\frac{\sum_{i=1}^{n}(T_{\mathrm{b},i}^{e} - T_{\mathrm{b},i}^{s})^{2}}{n}} \tag{3.3}$$

with n the number of calculated values for the temperature at each simulation, which depends on the evaluation step time.

Results are shown in Fig. 3.5. In order to quantify the accuracy of the optimal value, the relative percentage error (Fig. 3.4) between the experimental and the simulated temperature related to that value is calculated, and it is

$$e_r = \frac{T_{\mathrm{b}}^{s} - T_{\mathrm{b}}^{e}}{T_{\mathrm{b}}^{e}}\,100 \tag{3.4}$$

Due to the lack of additional experimental data, validation phase for the model in exam has not been performed and thus cabin model has not been used during the simulations.

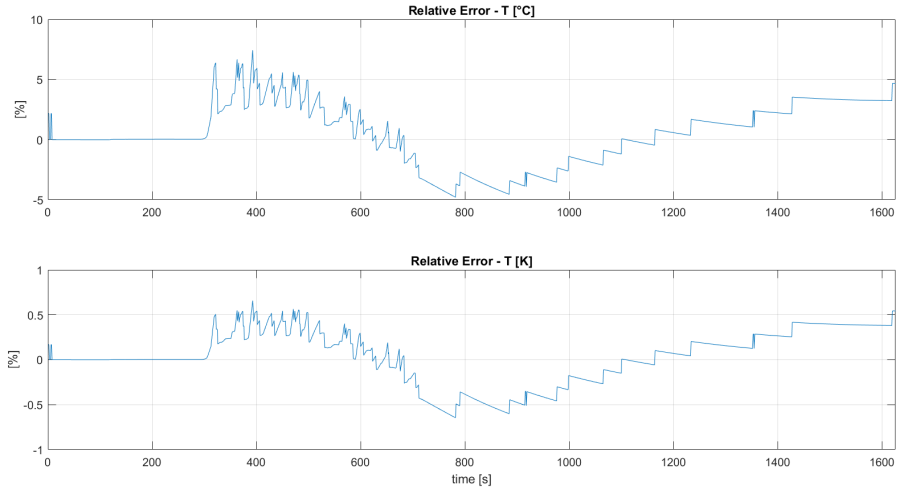

Figure 3.4: Relative error between the experimental and simulated battery temperature.

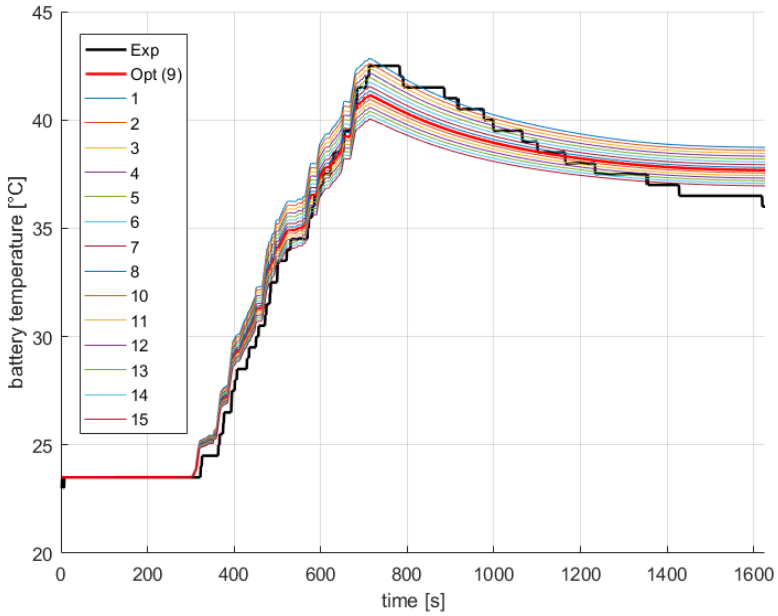

(a) Battery specific heat capacity calibration.

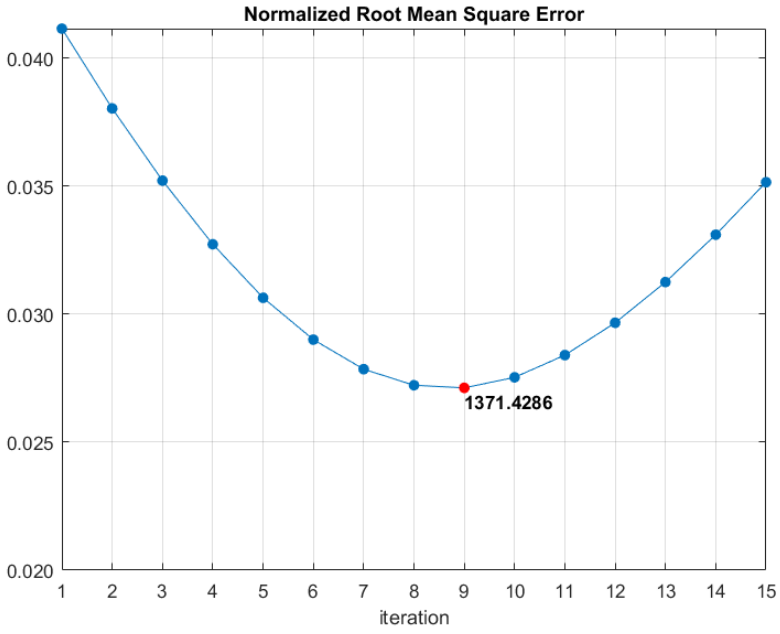

(b) NRMSE behaviour for each iteration of calibration.

Figure 3.5: Calibration of the battery cooling circuit model.

3.3 Energy-based cabin thermal model

As discussed in Ch. 2, cabin cooling and heating play an important role in thermal management control because of the intensive request for electric power to the high voltage battery. Therefore, a cabin thermal model is strictly necessary to take into account its effects on the battery temperature behaviour.

Objectives

The main aim of this modelling phase consists in the development of a simplified cabin thermal model, in which heat power losses between the cabin and the external environment are taken into account. The model focuses on the evaluation of cabin thermal needs in order to properly compute the electrical power request of the heating, ventilating and air-conditioning (HVAC) system.

In particular, the cooling system is composed by an electric compressor refrigerant cycle circuit in which heat exchange between refrigerant and cabin incoming air is performed at evaporator side (under dashboard), while refrigerant is cooled down by frontal air at condenser side (under-hood).

Different types of cabin models are proposed in literature.

One of the these are *CFD models* and they usually focus on cabin thermal comfort, thermal flows and heat distribution inside the cabin [15] and thermal effects of several cabin configurations such as windows opening or components materials. *Lumped-parameters models*, also called *mono-zonal models* have been developed [16, 17], as well. The cabin air is modelled using a single node and so the model can be considered homogeneous, i.e. internal air temperature is considered a time-depending parameter, not varying among the spacial domain defined by the cabin. Here, heat transfer analysis is performed by means of a theoretical approach, which usually comprehends convection and radiation equations as well as thermal inertia. A physical approach can be pursued, too, with the aid of a dedicated simulation software such as AMESim [18].

Development

The implementation of an integrated battery-HVAC system model would require a high developing effort as well as a non-negligible computational load during the simulation phase due the advanced submodels of the air-conditioning library. Moreover, because of only the energy evaluation requirements have to be fulfilled, a simplified model based on the mono-zonal approach is investigated and developed.

Thermal balance inside the cabin gives

$$\frac{dT_{\text{cab}}}{dt} = \frac{1}{m_{\text{air},in}\, c_{p_{\text{cab}}}} \left(\frac{dQ_{\text{HVAC}}}{dt} - \dot{Q}_{\text{los}} \right) \tag{3.5}$$

where dQ_{HVAC}/dt is the heat flow from the HVAC system to the cabin,, $\dot{Q}_{\text{los}}$ is the total thermal power losses, $m_{\text{air},in}$ is the air mass inside the cabin, $c_{p_{\text{CAB}}}$ is the equivalent heat specific capacity of the cabin, T_{cab} is the effective air temperature inside the cabin.

In this case, the narrow range of variation of the cabin temperature allows to assume $c_{p_{\text{cab}}} = \text{const.}$. Cabin thermal power losses according to [18] are considered. This study implements an AMESim advanced cabin thermal model for mid-size vehicle which takes into account the heat transfer between the cabin and the external environment through windshield, side windows, rearshield, side panels and roof. The behaviour of the cabin heat flows in different ambient temperatures are shown in Fig. 3.6.

Moreover, heat flow rate provided by the HVAC system depends on the ambient temperature and cabin temperature offset, $T_{\text{cab},os}$, i.e. the difference between the current cabin temperature and the target one. Although driver can set either manually or automatically the target value of cabin temperature, in the present model this boundary parameter is set to the constant value $T_{\text{cab},t} = 20℃$. The HVAC system is designed in such a way that

$$\dot{Q}_{\text{HVAC}} = \begin{cases} \dot{Q}_{max} = 4\,\text{kW}, & \text{if } T_{\text{cab},os} = 20℃, \\ \dot{Q}_{min} = \dot{Q}_{\text{LOS}}, & \text{if } T_{\text{cab},os} = 0℃. \end{cases} \tag{3.6}$$

This means that the maximum heating or cooling power $\dot{Q}_{max}$ is supplied when a threshold value for the offset temperature is reached. This value affects the HVAC

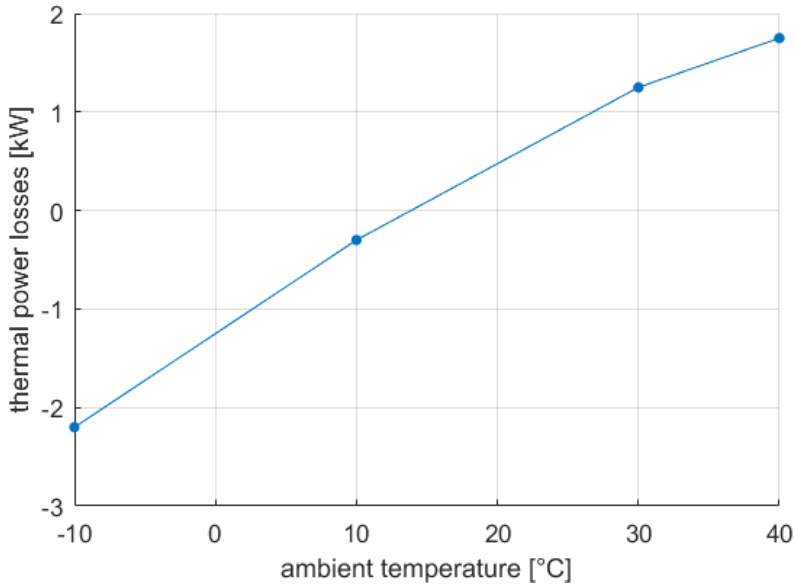

Figure 3.6: Total heat power losses between the cabin and the external environment in different ambient temperatures [18].

system design specifications. Once the reference target temperature is attained, the HVAC system has only to balance the cabin thermal power losses.

Moreover, standstill effects on cabin initial temperature are considered, as well. In order to analyse cabin thermal behaviour in this particular condition, the AMESim cabin model was employed. It was developed in the first part of the thesis project which was focused on the modelling of a HVAC system composed by an electric compressor, a condenser, an evaporator, a short-orifice tube and an accumulator, as suggested in [18], too. A summer and a winter scenario are considered. In Tab. 3.1, parameters for each test conditions are listed, which are: ambient temperature, T_{amb}, cabin wall temperature, T_{wall}, and solar irradiance, I_s [19]. Steady-state values of cabin temperature due to the standstill phase are listed, as well.

In Fig. 3.7, cabin temperature behaviour as a function of ambient temperature is depicted. Moreover, it follows that a standstill time of two hours is thus an adequate value in order to attain cabin thermal balance.

Table 3.1: Test conditions and cabin steady-state temperature values due to a 2 hours standstill phase.

Scenario	T_{amb} [°C]	T_{wall} [°C]	I_s [W/m²]	$T_{cab,ss}$ [°C]
winter	0	0	50	3.0
	10	10	100	15.3
summer	25	25	300	38.0
	35	35	400	51.5

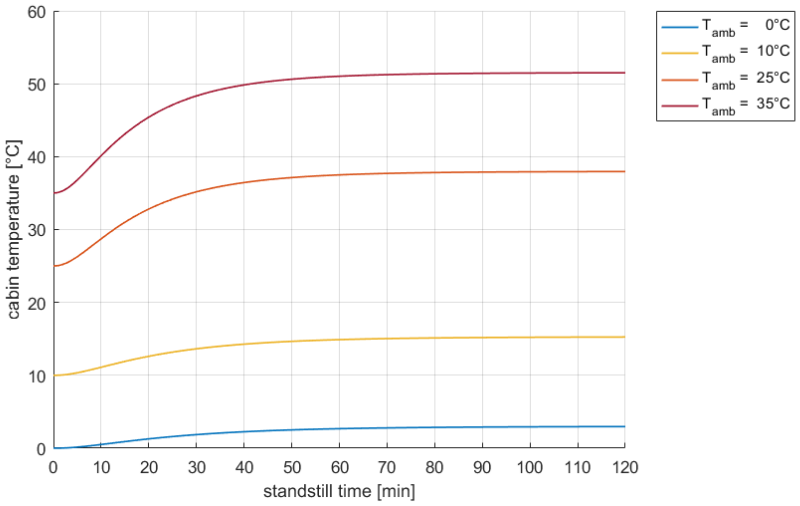

Figure 3.7: Cabin temperature as a function of standstill time and ambient temperature.

3.4 Models implementation and software co-simulation

All the 4 cooling circuit models developed in AMESim environment have been implemented in Simulink environment. This solution is adopted because of the vehicle analytical model and control already exists in the latter environment. Although the ICE model has been implemented, it hasn't been employed during the performed simulations because of its limited reliability due to a lack of experimental data which compromised model calibration. Thus, ultimately, the current status of the developed models is summarized in Tab. 3.2.

Table 3.2: Current status of the developed models.

Model	Developing environment	Imported in Simulink	Working	Employed
Battery c. c. m.	AMESim	yes	yes	yes
Front-axle c. c. m.	AMESim	yes	yes	yes
ISG c. c. m.	AMESim	yes	yes	yes
Engine c. c. m.	AMESim	yes	no	no
Cabin m.	Simulink	—	no	no

c. c.: cooling circuit; *m.*: model

Two ways of using AMESim models in Simulink environment can be followed: *Co-Simulation* and *Model Exchange*. The main difference between these approaches regards the used solver, which in the first case is the AMESim solver, while in the latter is the Simulink one. As explained in [14], it is not advised to use model exchange mode because it is considered deprecated and thus not reliable for models implementation. Therefore, co-simulation approach (Fig. 3.8) has been chosen. In this case, the only variables exchanged are the input and output variables and the rate of exchange is set according to a user-defined parameter. As the name indicates, the model is not entirely in the hands of a single piece of software (Simulink) but it is a co-operation between two (or more) software packages. It is important to realize that there is a loss of information by exchanging only input and output variables at a given sample rate. Thus, a sample rate of 1 second has been set, consistent to the slow thermal dynamics of the modelled components.

With regard to the chosen co/simulation mode, the Amesim to Simulink interface enables to convert the physical model to a Simulink S-Function (Fig. 3.9a), which can then be imported into Simulink and used within a Simulink system just like any other S-Function. The interface is designed so that many of the Amesim facilities can be used while the model is running in Simulink. In particular, parameters of the physical model can be changed within the Simulink environment with a user-friendly interface (Fig. 3.9b).

The employed simulation environment is represented by a *Model-in-the-Loop* system. The latter is employed in the context of Model-Based Design (MBD), a method

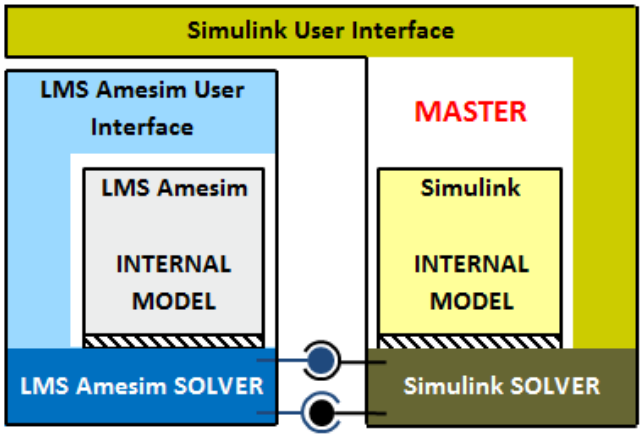

Figure 3.8: AMESim-Simulink co-simulation operating mode.

of addressing problems associated with designing complex control, signal processing and communication systems. Model-in-the-Loop helps to identify functional and non-functional issues in the early development stage, when verification complexity is relatively lower than that of the final systems, in order to verify the accuracy and acceptability using plant model of a control algorithm.

The architecture of the adopted MiL is such as to keep separated vehicle controls from physical components. For this purpose, it is organised in a two-tier system represented by

- a *Controller* block
  comprehends all the control algorithms related to each modelled vehicle component. The developed Rule-Based and eHorizon strategies are included, as well;

- a *Physical* block
  analytical and physical models are here implemented, including the thermal management control-oriented models (Fig. A.6).

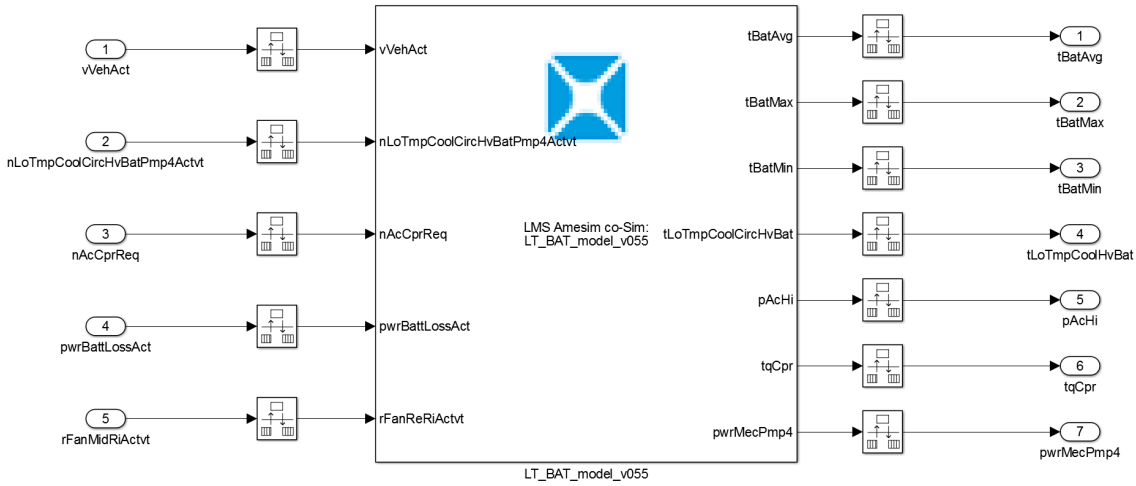

(a) Battery cooling circuit S-function block.

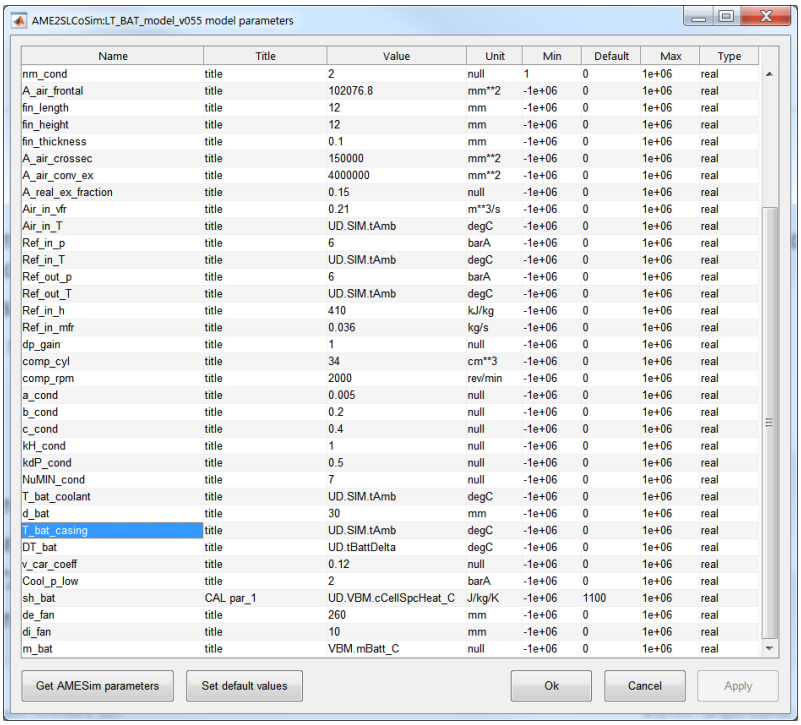

(b) Model parameters setting.

Figure 3.9: AMESim physical models implementation in Simulink environment.

Chapter 4

Development of the thermal management control strategies

In this chapter, the rule-based functions for the cooling systems are firstly explained. In particular, the control strategies of each cooling circuit actuators are investigated in order to clarify the Boolean conditions behind the functions.

Then, the eHorizon strategy is developed, with particular attention to the predictive thermal management control function. It takes into account several inputs such as speed and slope profile in order to estimate battery temperature behaviour over a well-defined time domain related to thermal relevant event. In this case, only city passages are considered and several assumptions are needed in order to identify the start and the end of each event. Analytical equations involving vehicle dynamics and battery thermodynamics are carefully explained, as well.

4.1 Rule-Based Strategies description

Heuristic thermal management is based on intuitive rules and correlations involving various parameters, principally temperatures.

One guiding principle of such a kind of strategy is to preserve the temperature of thermal-stressed components inside a restricted range of values, which are defined upon maximum efficiency consideration. In order to achieve this objective, upper and lower threshold temperatures are set after a calibration phase, which can turns out

to be an expensive task because of the choice of the best values is influenced by the architecture of the examined cooling system. Despite this disadvantage, heuristic control strategies are widely used in real-time controllers due to the low computational effort required. However, the lack of an analytical approach makes these strategies not to perform optimal control from an energy-efficiency standpoint.

Two common approaches to implement these intuitive principles are the *map-based* and the *rule-based* approach. In the map-based approach, the output set-points are stored in multi-dimensional maps whose entries are the measured parameters on which control is based. In the rule-based approach, several boolean conditions are verified at each calculation task in order to establish if the activation of the actuator is either needed or not.

The actuators involved in the developed heuristic control strategies are

- pumps
  their control strategies follow the rule-based approach in order to prevent components to reach too much high temperatures;

- high voltage compressor
  it is controlled with the same approach of the pumps, with the only difference that in this case several physical constrains are taken into account;

- fans
  their control strategies follow the map-based approach and are focused on coolant hot temperatures, i.e. the measured downstream the component to be cooled down.

The rule-based control strategy of the battery cooling circuit pump is shown in Fig. 4.1 by means of a flow chart and in Fig. 4.2 where battery temperature is compared to the fixed threshold values related to pump activity.

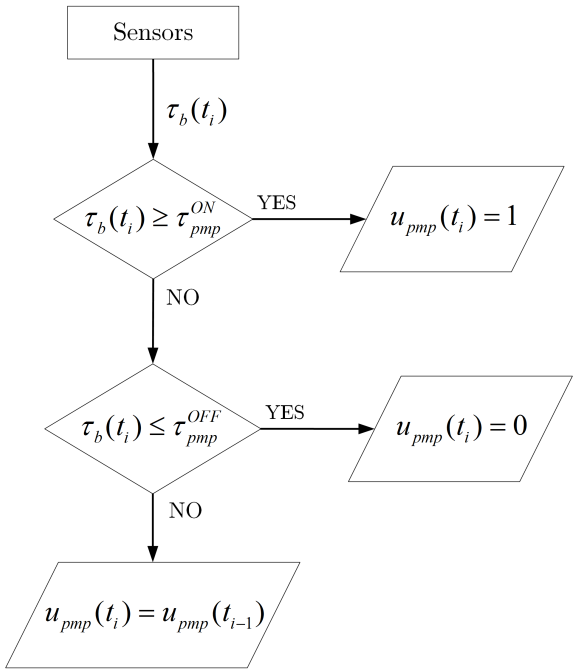

Figure 4.1: Flowchart for battery cooling circuit pump according to rule-based control strategy.

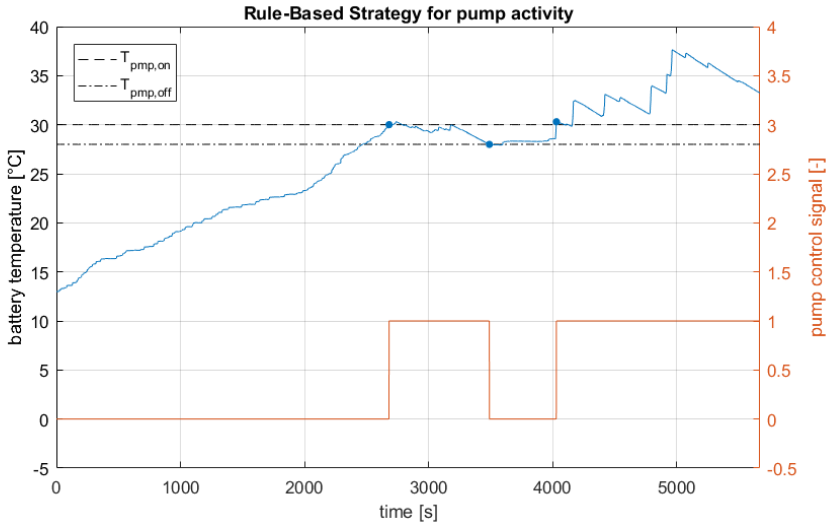

Figure 4.2: Rule-based control strategy for the battery cooling circuit pump.

4.2 eHorizon Strategy development

In this section, the development of the eHorizon Strategy is discussed.

Firstly, the architecture of the eHorizon Control Unit is described, taking into account a possible in-vehicle implementation using ADAS provider. Then, an algorithm developed in order to identify city passages in advance is presented. With the knowledge of this information, a predictive thermal management control function has been developed, as explained in the last section.

4.2.1 Architecture

As explained in Ch. 1, recent passenger cars are implemented with automobile build-in navigation systems. A state-of-the-art approach is to employ an electronic horizon provider, which provides several routing information [20].

Nevertheless, in real-world driving is not possible to know a priori the speed profile of the vehicle using only map data. Consequently, a *driver model* must be implemented in the eHorizon Control Unit (eHCU) in order to predict the velocity of the car in each segment of the planned route. The model could be developed in a way that driver behaviour is taken into account [20]. As a result, a predicted vehicle speed trajectory for real-world driving cycle can be obtained. This kind of approach is represented in Fig. 4.3a. Moreover, the data provided by the geographical information system (GIS) can be used to detect important thermal-related events, such as relevant slope sections and city passage. The latter has been here taken into account and examined for function development.

Since e-horizon provider and map database haven't been implemented in the simulation environment used for this activity, a modern navigation system couldn't be recreated. In order to overcome, this issue, a RDE cycle has been used instead. Speed limits have been reconstructed from the speed profile by mean of a City Detection Algorithm (CDA).

4.2.2 City Detection Algorithm

As mentioned above, the reason why such an algorithm was needed is the lack of routing information, except for speed and slope trajectories. Thus, the speed profile

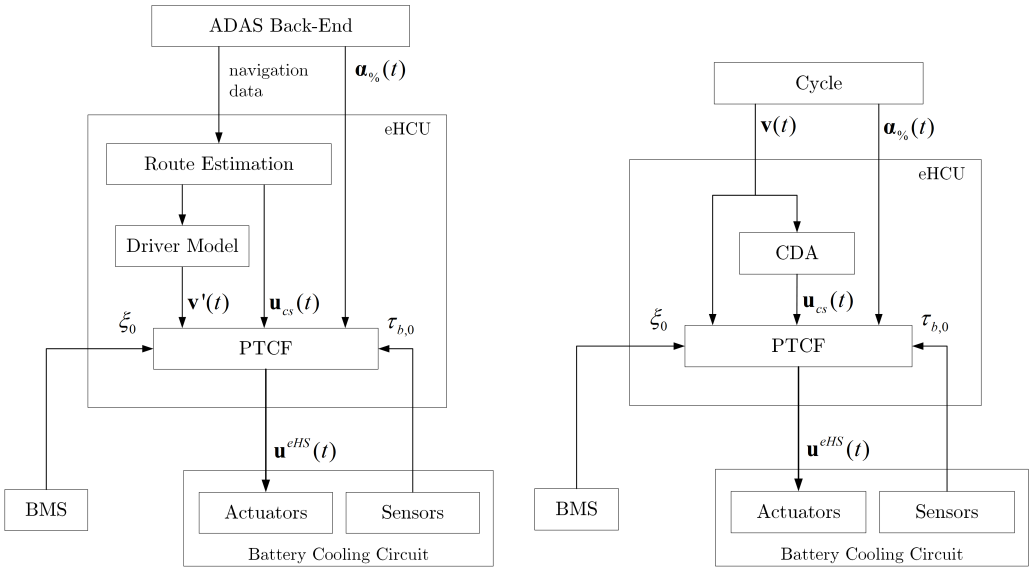

(a) On-board architecture. **(b)** Simulation architecture.

Figure 4.3: Comparison between a possible in-vehicle function architecture and the one employed for function development.

is examined to deduce speed limit values at each time instant and then assign a road category. The development of the algorithm is focused on a RDE cycle located in Bologna (Fig. A.1), which means that a prearranged pattern of road categories is pursued.

The main objective of the algorithm is recognizing city road type in order to establish

- *time instants* related to city enters
  at which the predictive thermal management function must perform the very first evaluation task

- *lengths of time* of city events
  which correspond to the operating window of the prediction function

The detection procedure is based on the following steps

STEP 1 Road index signal reconstruction (speed limits - based)
the speed profile input signal is analysed in order to establish trip patterns, which are categorised by road indices as shown in Tab. 4.1 Initially, the as-

Table 4.1: Speed limits for road sections.

Road index	Road type	Speed limits [km/h]
1	Urban	60
2	Rural	90
3	Motorway	130

signment of road indices is only based on speed limits. The output of this step is a time-based road index signal (Fig. 4.8);

STEP 2 Road index signal filtering

The aforementioned signal must be filtered in order to generate a homogeneous and coherent one with the RDE pattern (urban-rural-motorway)(Fig. 4.8);

STEP 3 - City square and trigger signals generation (Fig. 4.5)

A city square signal is generated in order to clearly identify the city event. In fact, the time instants related to city enter and exit and the city event time extension are evaluated. The distances to the city enter and exit and the city event length are evaluated, as well. Then, a city trigger signal is obtained from the previous one in order to serve as an enabling signal for thermal/energy management functions.

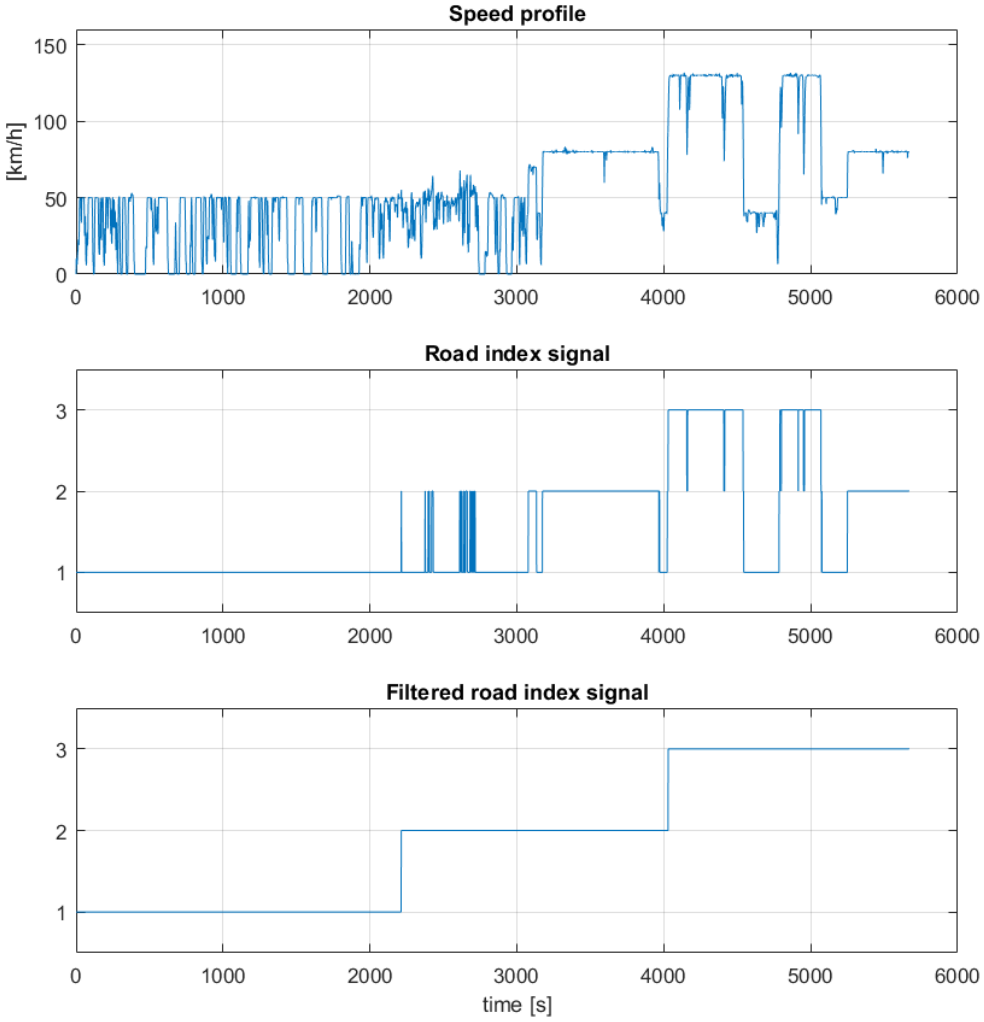

Figure 4.4: Speed profile and road type assignment.

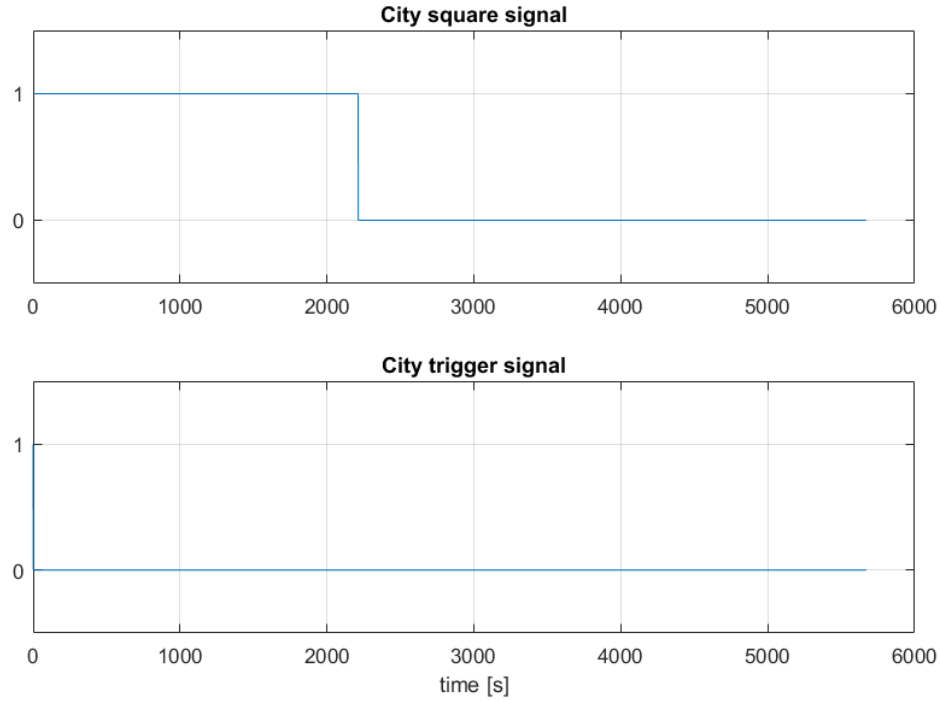

Figure 4.5: CDA output signals for event defining and first function task triggering.

4.2.3 Predictive Thermal management Control Function

The informations provided by the city detection algorithm are the input of the predictive thermal management control function, which has been developed for the battery cooling circuit. It takes into account the following signal and parameters:

- *input signals*, $i(t)$
  speed $v(t)$ and slope $s_l(t)$ profile

- *state variables*, $x(t)$
  high voltage battery temperature, τ_b

- *control signals*, $u(t)$
  compressor, $b_\mathrm{cpr}(t)$, and pump, $b_\mathrm{pmp}(t)$, control bit

Initial conditions must be set in order to perform the temperature prediction, as well. In this case, the values of battery state of charge, ξ_0, and temperature, $\tau_{\mathrm{b},0}$, at each function callback are needed.

Moreover, several *local constraints* are taken into account. They mainly regard physical parameters such as the maximum torque and power supplied by the electric machines and the operating window of the state of charge. In the latter case, this domain strictly depends on the type of the vehicle (HEV, PHEV, BEV) and consequently on the driving mode. As explained in § 4.2.2, only city events are considered to be thermal relevant in this project. Moreover, it is assumed that the city passage is always driven in pure electric and, since the vehicle in exam is a PHEV, it is in charge-depleting mode. Thus, although the initial state of charge ξ_0 at each task obviously depends on battery usage, namely the power request, its value at city enter is fixed. The latter is provided by powertrain energy management control in such a manner to make the driver capable to cover the entire distance of the chosen trip in electric drive. On the base of the trip knowledge, this target could be achieved by means of a specific electronic horizon function aimed at the optimization of the instantaneous split factor, $u(t)$, satisfying the power demand of the drive line in the most energy-efficient way (see: Ch. 6).

The analytical equations concerning vehicle powertrain and high voltage battery for temperature prediction are as follows.

Analytical equations

As previously explained, the topology of the considered PHEV is P1-P4. In particular, P4 architecture means the usage of two different motors, directly connected with the wheels. In this case, they are positioned on the front axle and although a transmission is mounted between the motors and the front wheels, its gear ratio is not considered as additional degree of freedom.

As shown in Fig. 4.6, the fundamental equation representing the longitudinal dynamics of a vehicle in motion is the following

$$m_{\mathrm{v}} \cdot \frac{d}{dt} v(t) = F_{mot}(t) - F_{res}(t) \tag{4.1}$$

where F_{mot} is the force supplied by the prime mover, here the electrical motors, and F_{res} is the resistant force acting on the vehicle. The latter can be expressed as follows

$$F_{res}(t) = F_a(t) + F_r(t) + F_g(t) + F_d(t) \tag{4.2}$$

and thus takes into account the effects of

- air resistance
  drag or aerodynamic force, F_a
- rolling resistance
  rolling force, F_r
- gradient resistance
  gravity force, F_g

air resistance (drag or aerodynamic force, F_a), rolling resistance (rolling force, F_r) and gradient resistance (gravity force, F_g), and all the other not specified effects (disturbance force, F_d). For the sake of simplicity, the latter is neglected.

Because of both air and rolling friction losses depend on vehicle speed, it is a matter of practicality considering drag and friction forces not separately. In particular, their contributions can be gathered in a single polynomial expression as a function of $v(t)$ with coefficients depending on the considered vehicle and which can be practically obtained by means of a *coast-down test*.

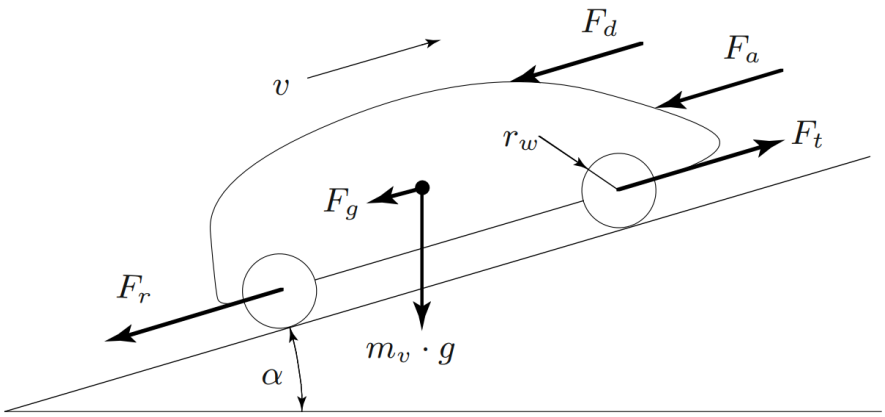

Figure 4.6: Forces acting on a vehicle in motion.

As explained in [21], the test consists in driving the vehicle in a flat road at a certain reference speed and then starting the coastdown deceleration phase, which means the transmission shall be in neutral and the engine shall run in idle. Moreover, the brakes shall not be operated during coasting. Experimental data of measured vehicle speed are then fit with a regression curve, namely the *total-resistance curve*, which has the following form

$$F_{cd}(t) = F_a(t) + F_r(t) = f_0 + f_1 \cdot v(t) + f_2 \cdot v^2(t) \tag{4.3}$$

where f_0 is the constant term [N], f_1 is the coefficient of the first-order term [N/(km/h)], f_2 is the coefficient of the second-order term [N/(km/h)^2].

The force induced by gravitational field on the vehicle when driving on a road with non-null gradient is as follows

$$F_g(t) = m_{\mathrm{v}} \cdot g \cdot \sin \alpha(t) \tag{4.4}$$

where $\alpha(t)$ is the slope angle [rad] of the road, which can be derived from percentage slope $\alpha_{\%}(t)$ by the relationship

$$\alpha(t) = \arctan \frac{\alpha_{\%}(t)}{100} \tag{4.5}$$

Hence, the resistant force has the following expression

$$F_{res}(t) = f_0 + f_1 \cdot v(t) + f_2 \cdot v^2(t) + m_{\mathrm{v}} \cdot g \cdot \sin\alpha(t) \tag{4.6}$$

By substitution of (4.3), (4.4) in (4.2), the fundamental equation (4.1) can be written in the form of an inhomogeneous first-order non-linear ODE

$$\frac{d}{dt}v(t) = k_0 + k_1 \cdot v(t) + k_2 \cdot v^2(t) + F_{mot}(t) \tag{4.7}$$

with obvious meaning of the coefficients k_i. Thus, the acceleration and the velocity of the vehicle, which represent the output of the vehicle model, can be evaluated from (4.7). Such a kind of approach is called *forward-facing* approach because of the source of the energy flow is represented by the mover and the sink corresponds to the wheels, at which velocity and acceleration are evaluated. These output signals are involved in a closed-loop control (using a PI controller) operated by an effective driver model with the role of following a target input signal, namely the speed profile of a certain driving cycle. Thus, this approach can includes dynamics effects and consequently performance- and drivability-focused simulation can be performed. The approach based on the inverted path of the energy flow inside the vehicle is called *backward-facing* approach. Here, the traction force, and consequently torque and power, are evaluated on the base of the vehicle speed, so there is no closed-loop control on the latter parameter, i.e. a driver model is not needed. Because of the main objective of the predictive function is represented by the evaluation of the battery power request, and thus the temperature behaviour, with no particular attention to the control of the traction torque in the interests of energy management optimization problems, the backward approach is used in the present activity.

Similarly to (4.1), torque balance applied to the front wheels gives:

$$T_{\mathrm{w}}(t) = T_{mot}(t) - T_{res}(t) = J_{eq} \cdot \frac{d}{dt}\omega_{\mathrm{w}}(t) \tag{4.8}$$

where T_{w} is the net torque applied to the wheels, T_{mot} is the overall torque request, T_{res} is the resistant torque acting on the vehicle, J_{eq} is the equivalent moment of inertia, i.e. reduced to the wheel, and ω_{w} is the revolution speed of the front wheels, which are considered to be the same for both of them.

The resistant torque is evaluated in correspondence of the front wheels, hence

$$T_{res}(t) = F_{res}(t) \cdot r_{\mathrm{w},f} \tag{4.9}$$

The equivalent inertia moment is evaluated by reducing the entire system (the vehicle) to the front and rear wheels; the system is assumed to be rigid, including the wheels. It is as follows

$$J_{eq} = J_{eq,f} + J_{eq,r} \tag{4.10}$$

where the quantities $J_{eq,f}$ and $J_{eq,r}$ are calculated by imposing the equivalence of the kinetic energies of the initial and the reduced system

$$E_{eq}(t) = E(t) \tag{4.11}$$

where for the front wheels one has

$$\begin{aligned} E_{eq}(t) &= \frac{1}{2}\, J_{eq,f}\, \omega_{\mathrm{w},f}^2(t) \\ E(t) &= \frac{1}{2}\, (2 \cdot J_{\mathrm{w},f})\, \omega_{\mathrm{w},f}^2(t) + \frac{1}{2}\, m_f\, v^2(t) \end{aligned} \tag{4.12}$$

where m_f is the front lumped mass of the vehicle, weighted on the distance of the front axle from the vehicle centre of gravity. Equation (4.12) yields

$$J_{eq,f} = 2J_{\mathrm{w},f} + m_f\, r_{\mathrm{w},f}^2 \tag{4.13}$$

and analogously for the rear wheels. Thus, the traction torque requested to the front wheels can be obtained from equation (4.8) as follows

$$T_{mot}(t) = T_{res}(t) + \left(\frac{J_{eq,f}}{r_{\mathrm{w},f}} + \frac{J_{eq,r}}{r_{\mathrm{w},r}} \right) \frac{d}{dt} v(t) \tag{4.14}$$

Because of the front motors can be used in regenerative braking as electric power generator in order to absorb the kinetic energy of the vehicle and thus to recharge the high voltage battery, the actuated motor torque, i.e. the torque applied upstream

of the transmission just before the wheels, can be

$$T_{\mathrm{tr}}(t) = \begin{cases} \frac{1}{\eta_{\mathrm{tr}}} \cdot \frac{T_{mot}(t)}{N_{\mathrm{m}}\,\gamma_{\mathrm{tr}}}, & \text{if } T_{mot}(t) >= 0 \text{ (traction)} \\ \eta_{\mathrm{tr}} \cdot \frac{T_{mot}(t)}{N_{\mathrm{m}}\,\gamma_{\mathrm{tr}}}, & \text{if } T_{mot}(t) < 0 \text{ (regenerative braking)} \end{cases} \tag{4.15}$$

where η_{tr} and γ_{tr} are the constant values for the mechanical efficiency and the gear ratio of the transmission, respectively, and N_{m} is the number of the traction motors (in this case mounted on the front axle), here 2 (P4 architecture). The balance of the actuated and requested torques applied to the motor gives

$$T_{\mathrm{m}}(t) - T_{\mathrm{tr}}(t) = J_{\mathrm{m}} \frac{d}{dt} \omega_{\mathrm{m}}(t) \tag{4.16}$$

where the motor revolution speed is calculated as $\omega_{\mathrm{m}}(t) = \omega_{\mathrm{tr}}(t) = \gamma_{\mathrm{tr}} \cdot \omega_{\mathrm{w}}(t)$. In order to quantify the efficiency of the motor-inverter group, a *power losses map* is employed to evaluate the electrical power losses of the motor in function of the requested torque and the revolution speed (generally expressed in rpm)

$$P_{\mathrm{m},los}(t) = f\left(T_{\mathrm{m}}(t), n_{\mathrm{m}}(t)\right) \tag{4.17}$$

Hence, the electrical power request of the motors can be written as

$$P_{\mathrm{m},el}(t) = P_{\mathrm{m},mec}(t) + P_{\mathrm{m},los}(t) \tag{4.18}$$

where $P_{\mathrm{m},mec}(t) = T_{\mathrm{m}}(t) \cdot \omega_{\mathrm{m}}(t)$ is the delivered mechanical power that can be either positive or negative in case of traction or regenerative braking, respectively, and the quantity $P_{\mathrm{m},los}(t)$ is obviously assumed to be strictly positive at each working point, according to (4.18).

The electric power requested to the high voltage battery is the sum of several contributions, which are

- the power of the electric machines
  in case of regenerative braking, the motor power request represents a negative demand to the battery, which means it gets charged by kinetic energy dissipation due to vehicle deceleration;

- the power of the DCDC converter for balancing the auxiliaries power request to the low voltage battery
  because of the low voltage battery must supply electric power to infotainment system, several actuators (such as the electric pumps of the cooling circuits) and other components (e.g. the headlights), its voltage is continuously maintained to a constant value (typically 12 V) thanks to the DCDC by power absorption from the traction battery;

- the power of the ISG
  in pure electric drive, a null power is requested from the ISG because of it is employed for traction purpose only in performance drive cycles, which is not the case of an RDE one. Moreover, due to the position of the traction motors on the front axle in the present hybrid topology, regenerating power during braking employing the P4 machines results in a more energy-efficient solution than using the ISG. For these reasons, ISG power contribution is not considered;

- the power amount of the high voltage compressor and the PTC cabin heater
  the first one is employed for the cooling of both the traction battery and the cabin, while the latter has the only purpose of cabin heating. As previously explained, cabin HVAC model is unavailable and thus the related power request is not to be considered. Concerning the battery cooling circuits, the power demand of the compressor isn't take into account because of the cooling power effects on battery temperature behaviour is not considered for a matter of simplicity of function development regarding heat transfers analytical modelling.

Hence, the requested battery power can be stated as follows

$$P_{\mathrm{b}}(t) = N_{\mathrm{m}}\, P_{\mathrm{m}}(t) + P_{\mathrm{dc}} \tag{4.19}$$

with $P_{\mathrm{dc}} = P_{\mathrm{aux}}/\eta_{\mathrm{dc}}$, where P_{aux} is the auxiliaries power request to low voltage battery and the converter electric efficiency η_{dc} is assumed to be constant.

In order to evaluate the temperature of the battery, the power losses, and consequently the electric current, must be firstly calculated.

The electric current has the following form

$$i_{\mathrm{b}}(t) = \frac{V_{\mathrm{b},oc}(t) - \sqrt{V_{\mathrm{b},oc}^2(t) - 4P_{\mathrm{b}}(t) \cdot R_{\mathrm{b}}(t)}}{2R_{\mathrm{b}}(t)} \tag{4.20}$$

where the open circuit voltage $V_{\mathrm{b},oc}(t)$ and internal resistance $R_{\mathrm{b}}(t)$ of the battery are evaluated on the base of the same quantities referred to the single cell as follows

$$V_{\mathrm{b},oc}(t) = N_{\mathrm{c},s} \cdot V_{\mathrm{c},oc}(\xi(t)) \tag{4.21}$$

$$R_{\mathrm{b}}(t) = \frac{N_{\mathrm{c},s}}{N_{\mathrm{c},p}} R_{\mathrm{c}}(\tau_{\mathrm{b}}(t)) \tag{4.22}$$

where $N_{\mathrm{c},s}$ and $N_{\mathrm{c},p}$ are the number of cells in series and parallel, respectively. The open circuit voltage and the internal resistance of the cell strictly depends on the state variables of the predictive function, i.e. the state of charge and the temperature of the battery, respectively.

The state of charge of the battery is defined as the ratio of the remaining capacity to the maximum available one. In symbols

$$\xi(t) = \frac{C_0 - C(t)}{C_{max}} \tag{4.23}$$

where $C_{max} = C_{\mathrm{c}} \cdot N_{\mathrm{c},tot}$ and $C_0 = \xi_0 \cdot C_{max}$ is the initial battery capacity intended as the maximum capacity weighted on the initial value of the SoC. Hence

$$\xi(t) = \xi_0 - \frac{N_{\mathrm{c},s} \int i_{\mathrm{b}}(t)\, dt}{C_{max}} \tag{4.24}$$

Electric power losses are simply defined as

$$P_{\mathrm{b},los}(t) = R_{\mathrm{b}}(t) \cdot i_{\mathrm{b}}^2(t) \tag{4.25}$$

and are responsible of battery heating (*Joule* or *resistive heating*). Neglecting the convective heat transfer between the battery and the surrounding air and not considering the cooling power supplied by the battery cooling circuit (as previously

explained), the thermal balance applied to the battery gives

$$\tau_{\mathrm{b}}(t) = \tau_{\mathrm{b},0} - \frac{P_{\mathrm{b},los}(t)}{m_{\mathrm{b}} \cdot c_{p,\mathrm{b}}} \tag{4.26}$$

where $\tau_{\mathrm{b},0} = \tau_{amb}$, i.e. the initial battery temperature corresponds to the ambient one, which represents an important environment constrain, as discussed in Ch. 5.

Calibration and validation

The behaviour of the state variables has been examined. The comparison between the effective and predicted battery state of charge and temperature are shown in Fig. 4.7 and Fig. 4.8, respectively. It can be seen that the SoC is affected by a not so high accuracy. This fact can be explained considering both the complexity of vehicle dynamics and the simplified analytical approach at the base of function development. Indeed, in order to achieve more accurate results, several control-based and physical-based constraints should have been implemented in the predictive function, such as torque wheel gradient limiter, torque smoothing during braking at low speeds, and battery peak and continuous power limits both in discharging and recharging.

Such a developing would have compromised the simplified approach on the base of which the function has been intended, with a consequent loss of generality essential for function application to others hybrid topologies. Moreover, because of the backward approach is followed and due to the importance of the prediction of the only battery temperature, the accuracy of the evaluated parameters can be considered acceptable.

In order to improve it, a remark can be made on the step size (equal to 1 s) of the evaluation task performed by the function, which is much higher than the one set for the Simulink vehicle model for a reason of computational effort reduction. This parameter might be considered for further step of function validation and calibration.

Working principle

The function is enabled by a trigger signal every time an event occurs, i.e. at city enter, in order to predict the temperature of the battery. Moreover, another

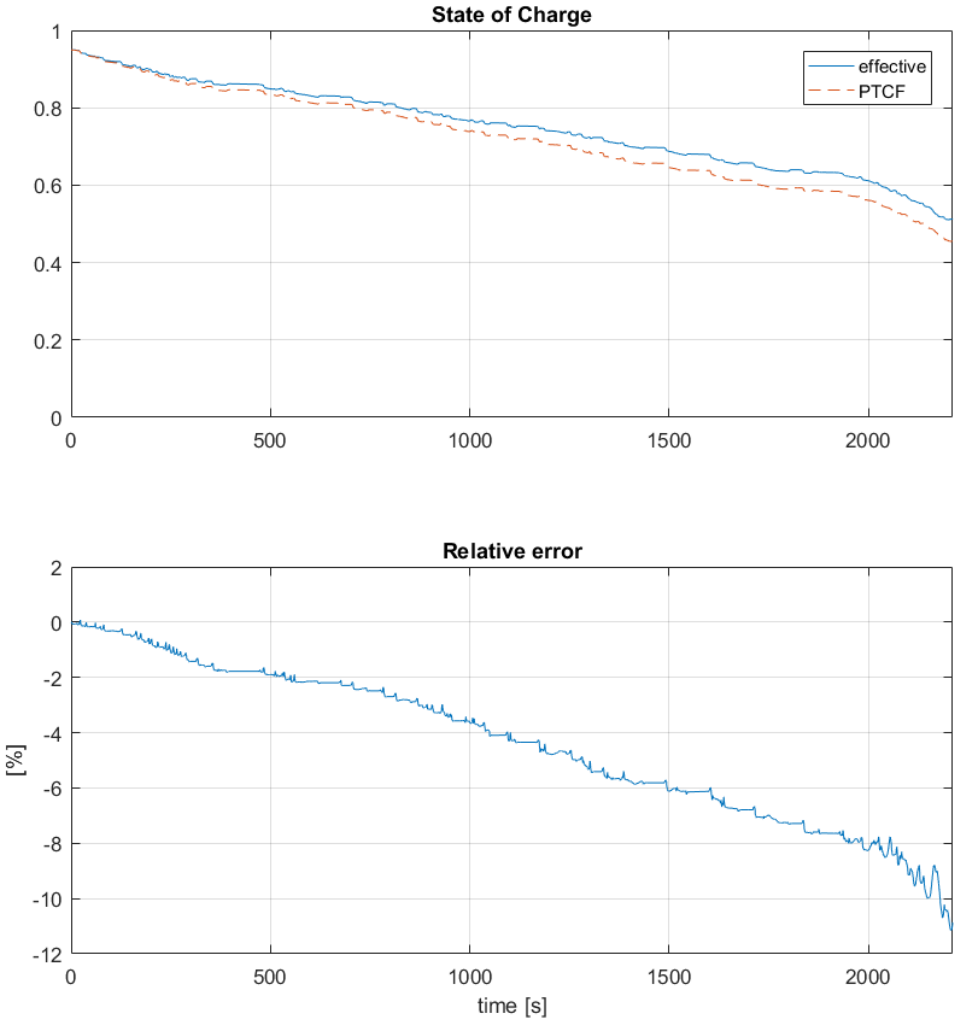

Figure 4.7: Comparison between the effective and predicted state of charge of the battery.

prediction task needs to be performed in the case of maximum battery temperature $\tau_{\mathrm{b},max}$ is higher than an upper limit value, established such as to avoid battery de-rating as well as ageing. According to [7], a reasonable value of the limit temperature could be $T_{\mathrm{b},ul} = 40$℃.

Depending on the driving cycle, namely the speed and the slope profile, and the ambient temperature, the two following situations can occur:

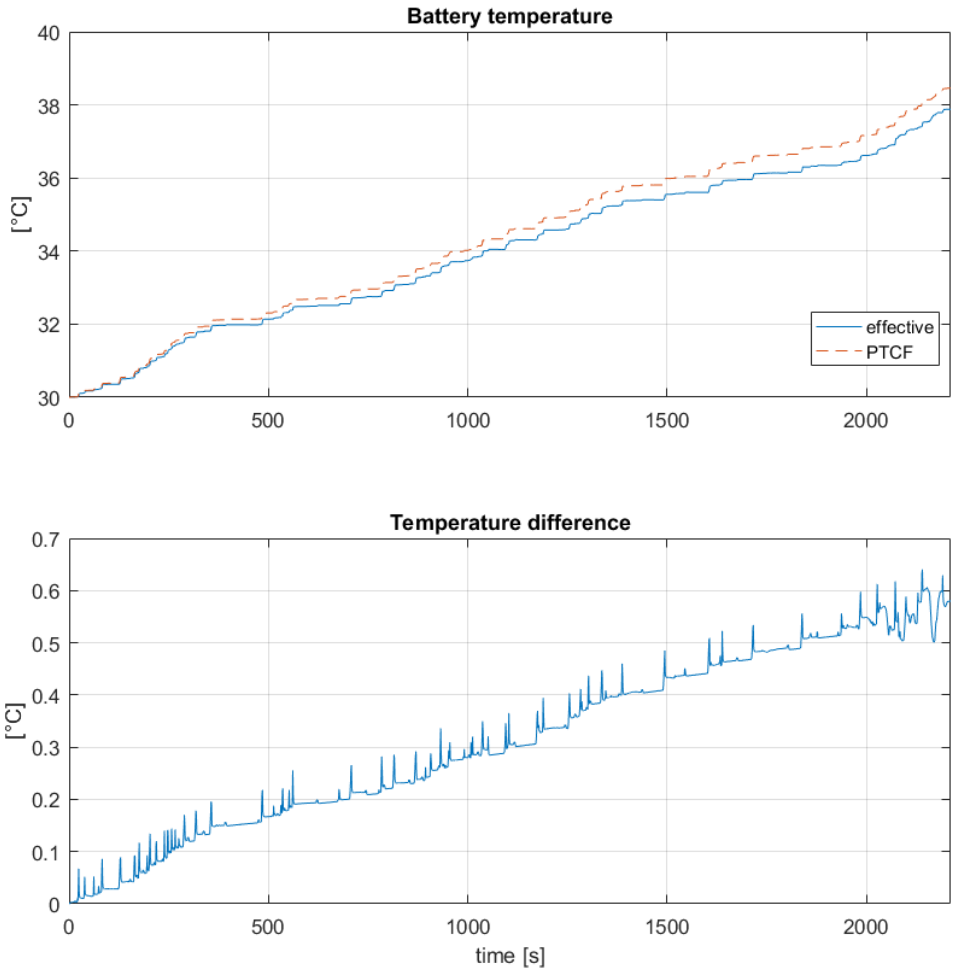

Figure 4.8: Comparison between the effective and predicted temperature of the battery.

1. $\tau_{\mathrm{b},max} \leq \tau_{\mathrm{b},lim}$
   the predicted maximum battery temperature does not exceed the imposed upper limit. This could be the case of

   - a trip performed in cold scenarios, in which the environment plays an important role to keep the battery cooled down due to favourable initial thermal conditions
   - a short trip, maybe due to a short city event or to a low initial value of

the SoC, which causes the battery not to satisfy a power request for such a long period to make the cooling required

Hence, battery SoH is not at risk and consequently cooling is not needed. The actuators of the battery cooling systems are not activated, even in the case in which the battery temperature has exceeded the upper limit value of the RBS to make the pump and the compressor switched on. The output signal of the predictive function are $b_{\text{cpr}}^{eHS} = b_{\text{pmp}}^{eHS} = 0$;

2. $\tau_{\text{b},max} > \tau_{\text{b},lim}$
the imposed upper limit temperature could be exceeded when

   - middle/high ambient temperature is present, causing the battery to reach faster a critical thermal condition
   - a long trip maybe combined with an aggressive driving and steep-sloped road sections

   Consequently, after the very first task the actuators are activated: $b_{\text{cpr}}^{eHS} = b_{\text{pmp}}^{eHS} = 1$.

Flowcharts related to temperature prediction and actuators control are depicted in Fig. 4.9 and Fig. 4.10, respectively.

The operating mode described in case (1) during a city passage in the RDE cycle located in Bologna is depicted in Fig. 4.11. In the latter case, because of in (4.26) the contribution of the absorbed heat by the coolant is not taken into account, several evaluation tasks are repetitively needed. This is the reason why discontinuities characterizing the predicted temperature behaviour can be observed. When the evaluation task is performed, the initial battery temperature corresponds to the actual one, which can be considered an initial varying constrain for each task. The main challenge of the predictive function is to apply the best thermal management control during the event. The target of the function is to minimize the difference of temperature between the effective battery maximum temperature and the upper limit one. Indeed, the closest is the battery temperature to the thermal limit, the less is the battery cooling request. Hence, in case (2) the eHorizon strategy activates the pump and the compressor at the event start and make the battery

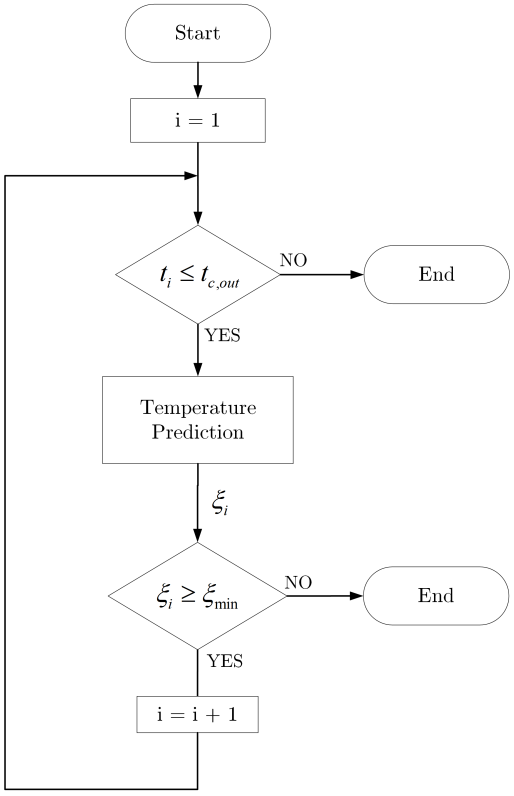

Figure 4.9: Flowchart for battery temperature prediction.

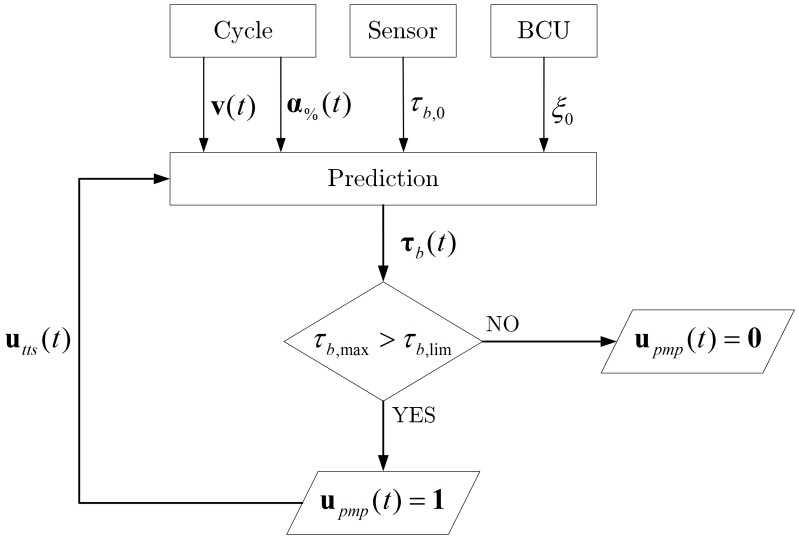

Figure 4.10: Flowchart for battery cooling system actuator control.

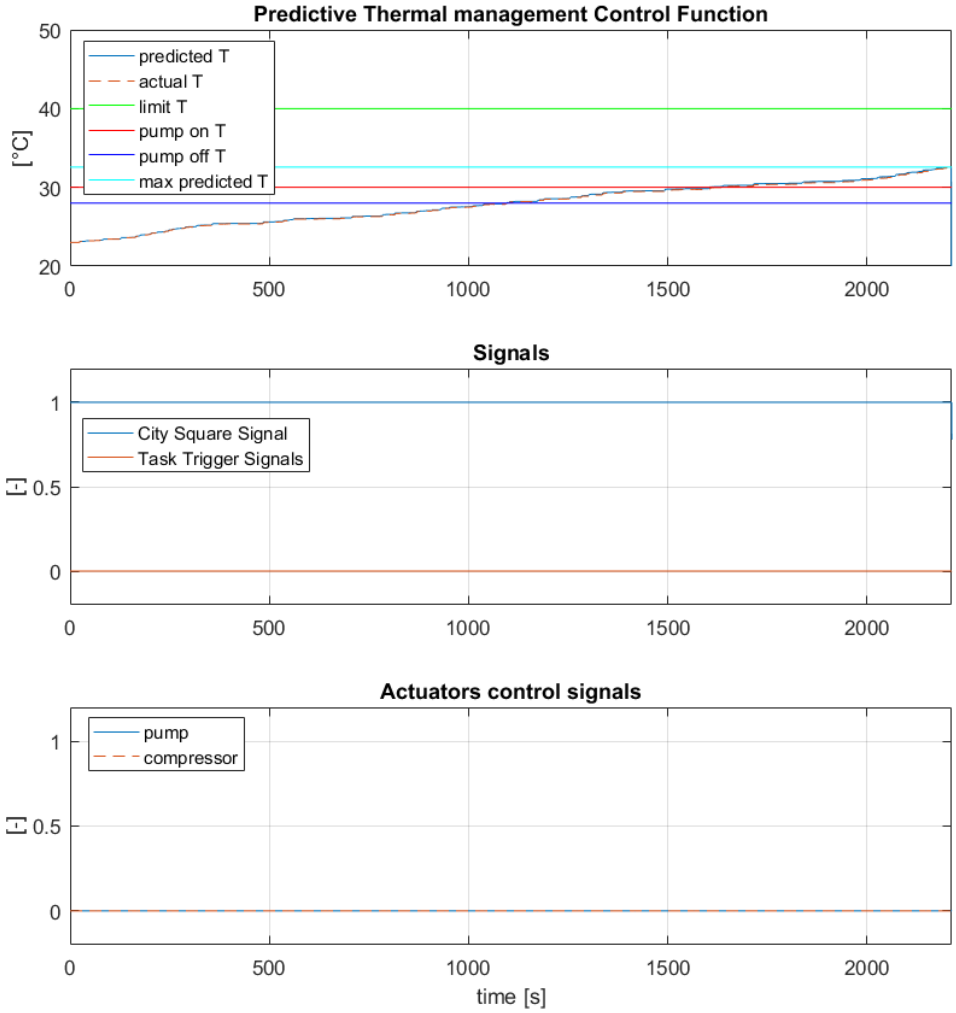

Figure 4.11: Function operating mode in case of no battery cooling request.

cooled down until its maximum predicted temperature is just right below the limit one. Moreover, an SoC monitoring is implemented in the function, as well. The purpose of this feature is taking into account the SoC behaviour during temperature prediction in order to establish the effective length of the horizon to be reconstructed. In case of an initial low value of the state of charge, city passage could not be completed. Therefore, the temperature of the battery is no more estimated over the time domain of the event, but considering the instant of time at which SoC drops

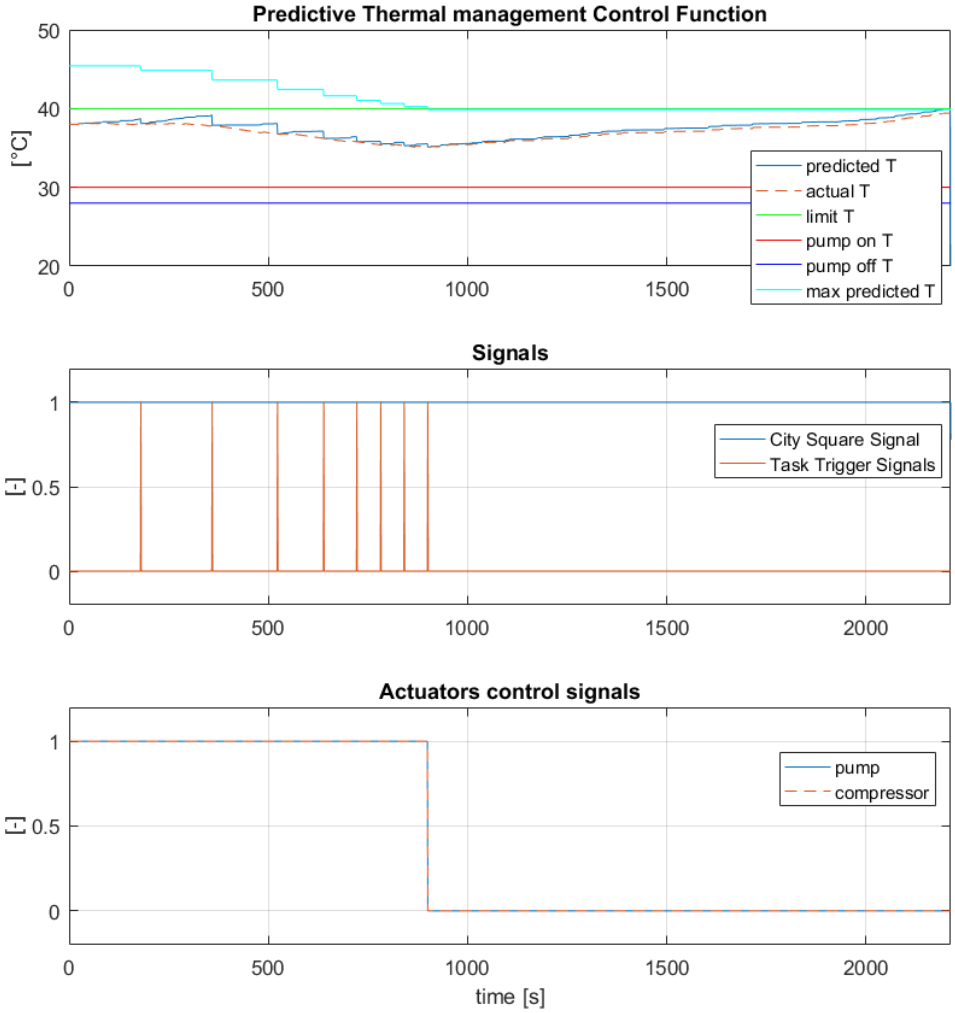

Figure 4.12: Function operating mode in case of battery cooling request.

below the lower limit value as the instant corresponding to city end. It can be said that the state of charge provides a *virtual event end*, which varies in function of the particular drive cycle and initial conditions.

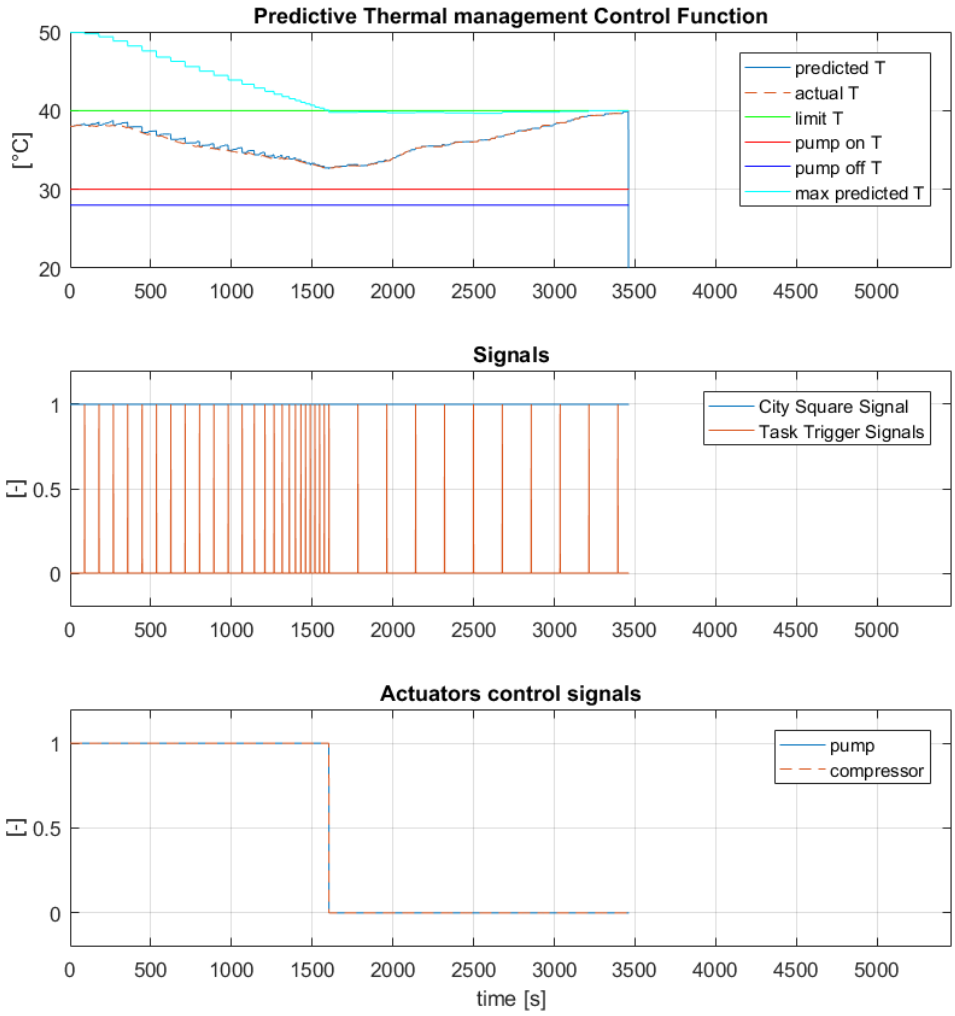

Figure 4.13: SoC monitoring in temperature prediction.

Chapter 5

Simulations and results

In this chapter, the results obtained comparing the Rule-Based and the eHorizon Strategy are presented and discussed. The behaviour of the state of charge, the all electric range (AER) and the fuel consumption (FC) are investigated in different ambient conditions.

5.1 Test cases and conditions

In order to prove and evaluate the advantages achieved by applying an eHorizon strategy instead of a rule-based one in the context of the thermal management control of the battery cooling circuit, a set of simulations has been designed.

The testing conditions mainly concern the environmental temperature, which value corresponds to the initial temperature of each component and fluid inside the pipelines of the cooling circuits. Because of the efficiency of the high-voltage battery, the electric motors and other thermal-stressed components depends on the their temperatures, an operating thermal range must be pursued and achieved not only for performances-based reasons, but also and above all for a matter of safety and, consequently, of preserving the service life of the component.

As explained in Ch. 1, because of the New European Driving Cycle (NEDC) is no more suitable for certifying exhaust emissions of light-duty vehicles, a RDE cycle has been used to perform the simulations. In particular, the same used in § 4.2 to validate the Predictive Thermal management Control Function is taken into

account.

A cabin thermal model has been developed and validated, as discussed in § 3.3. Nevertheless, the HVAC system has been disabled in each simulation in order to consider the only effects of the environmental temperature on the investigated parameters.

The main objectives of the performed set of simulations is to compare the method of operating of the aforementioned strategies by analysing and comparing the results obtained for the following parameters

- State of Charge
  because of cooling circuits require power to the high-voltage battery, an energy-efficiency thermal management control should minimize the battery energy consumption which is expressed in terms of SoC, as evaluated in (4.24), § 4.2;

- All-Electric Range
  the AER represents the distance covered by the vehicle using only the traction power provided by the electric battery pack, before the ICE is to be switched on. Hence, it starts at the beginning of the test cycle (i.e. at vehicle ignition) and ends at the first engine ignition, due to the energy management control strategy applied by the Hybrid Control Unit (HCU). Because of this supervisor control unit makes this decision upon a minimum threshold level of the SoC, the latter and the AER are deeply correlated;

- Fuel Consumption
  because of this parameter is related to engine activity, FC is expected to vary proportionally to the AER for a given torque split control strategy.

In order to investigate the behaviour of these parameters as a function of the environmental temperature and the applied thermal management strategy, the following test cases are proposed

Test case 1 city passage
the first section of the RDE cycle corresponding to the city event is performed in electric drive. The aim here is to compare the results for the SoC at city exit;

Test case 2 full RDE cycle

the whole drive cycle is simulated and charge-depleting and -sustaining modes are sequentially applied, according to PHEVs operating strategy. As discussed in § 4.2, the PTCF has been developed considering the high-voltage battery as the only traction power source of the vehicle. Hence, the eHS is applied only in charge-depleting mode, and then the RBS applies;

Test case 3 full RDE cycle with null slope

the whole drive cycle is performed one again imposing a zero slope profile. As will be shown and discussed later on in § 5.3, the road gradient has an intensive and non-negligible impact on the resistant torque.

The test cases and conditions related to the simulations' set are summarized in the following test matrix (5.1).

Table 5.1: Test matrix regarding the performed set of simulations.

Test cases	T_{amb} [°C]	ξ_0 [%]	**Strategy applied**	**No. of simulations**
1) city passage 2) full RDE cycle 3) full RDE cycle with null slope	10, 20, 30, 35, 40, 45, 50	95	RBS, eHS	14

A wide ambient temperature range is covered in order to observe in detail the operating of both the strategies and their impact on the investigated parameters. The initial value $\xi_0 = 95$ % for the state of charge was chosen for the simulations' set because of the relevant thermal inertia of battery cooling and heating phenomena.

Let $a(T_{\text{amb}})$ be the generic investigated parameter as a function of the initial environmental condition. For each test case, normalized values of the parameter are listed, and they are evaluated as follows

$$a(T_{\text{amb}}) = \frac{a(T_{\text{amb}})}{\max(a^{RBS}, a^{eHS})}\, 100 \tag{5.1}$$

5.2 Test case 1 – City passage

In this test case, the driving mode is forced in pure electric and the eHorizon strategy is active for all the trip long, when applied.

The behaviour of the maximum temperature and the SoC of the battery are depicted in Fig. 5.2 and Fig. 5.3, respectively.

As can be seen in Fig. 5.3, the vehicle is able to perform the whole city passage in pure electric mode with both the strategies applied and at every environmental test condition.

Concerning battery maximum temperature, when eHorizon strategy applies, the thermal management control acts in order to minimize the difference $\Delta T_{\mathrm{b}} = T_{\mathrm{b},lim} - T_{\mathrm{b},max}$ at city exit, as depicted in Fig. 5.2. Basing upon the PTCF working principle, the lower is this temperature difference, the lower is the duty period of the battery cooling system actuators. Therefore, once the pump and the high-voltage circuit are activated at the beginning of the event, if battery cooling is needed, the eHS is able to achieve the energy-efficiency target by switching off the actuators when the temperature target is accomplished.

With regard to the behaviour of the state of charge as a function of ambient temperature, it can be expected that the major advantages of the eHS in terms of SoC values at city exit will take place at middle temperatures. The reason why this should occur is that at low ($T_{\mathrm{amb}} \leq 10$℃) and high ambient temperatures ($T_{\mathrm{amb}} \geq 50$℃) battery cooling is never or always demanded, respectively, by both the strategies. The expected advantages of the eHS are hereby confirmed in Tab. 5.2, which indicates that the state of charge of the battery at city exit obtained by applying the predictive strategy is always higher than the one reached by the RBS, except for extreme temperatures. The highest benefit is reached at $T_{\mathrm{amb}} = 30$℃.

Therefore, the value of SoC is supposed to decrease with increasing environmental temperatures because of a growing amount of thermal power must be absorbed from the battery by the cooling circuit. Nevertheless, one might notice that this trend is not verified at $T_{\mathrm{amb}} = 20$℃ for the eHS and at $T_{\mathrm{amb}} = 50$℃ for both the strategies.

In the first case, this can be explained by considering the decreasing behaviour of the cell internal resistance as a function of its temperature and then of the environmental one. The higher is the battery temperature, the lower are the internal

Table 5.2: Test Case 1 – Results for the state of charge at city exit.

T_{amb} [°C]	$\xi_{\mathrm{c},in}$ [%]	$\xi_{\mathrm{c},out}^{RBS}$ [%]	$\xi_{\mathrm{c},out}^{eHS}$ [%]
10	95	98.2	98.2
20	95	96.9	100.0
30	95	88.0	98.8
35	95	85.2	94.5
40	95	84.5	90.3
45	95	83.0	85.5
50	95	88.8	88.8

resistance and then the power losses, but at the same time the higher is the cooling power request. From an energetic point of view, the obtained results show that in the range $T_{\mathrm{amb}} \in [10{,}30]$ [℃] the positive effect of ambient temperature on power losses reduction is greater than the negative one related to the increasing amount of heat power to be absorbed from the battery. In particular, the major benefit of this tread-off is achieved at $T_{\mathrm{amb}} = 20$℃, at which the value of the battery internal resistance is relatively low and no cooling power needs to be supplied, according to the operating mode of the predictive function.

Moreover, the higher values of SoC at city exit at very high temperatures ($T_{\mathrm{amb}} = 50$℃) are related to the compressor control strategy, which acts on the component speed in order to avoid dangerous excess pressures due to the high temperature of the refrigerant. When its pressure exceeds an upper threshold, the compressor is switched off and then on only when a lower pressure value is reached. This is due to the fact that the component was not designed to absorb such a high thermal power related to extremely high environmental temperatures. As a result, the overall activity period of the compressor can be shorter, even if a major cooling power is requested at higher ambient temperatures. Therefore, the total amount of battery energy consumption due to the compressor activity starts to reduce over $T_{\mathrm{amb}} > 45$℃ (Fig. 5.1).

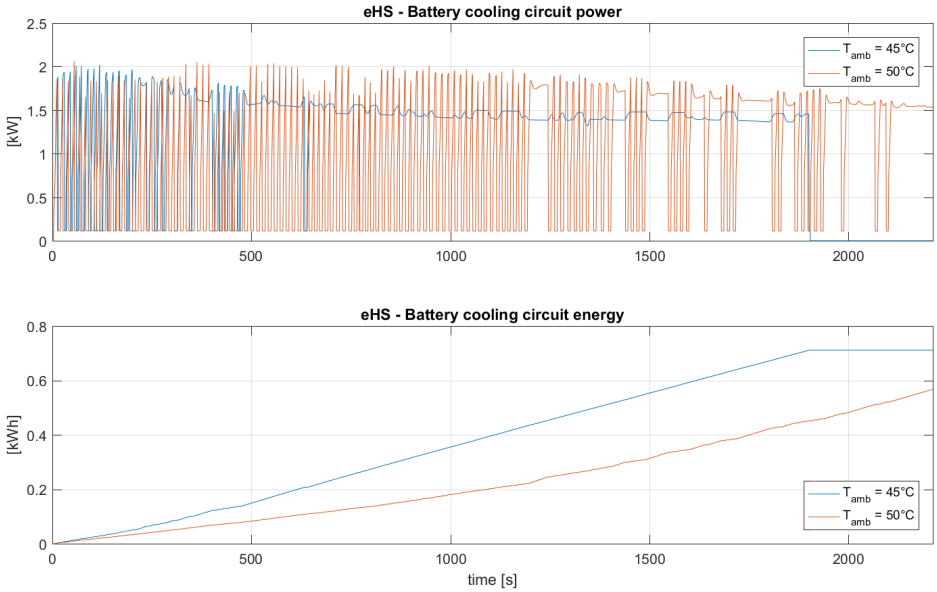

Figure 5.1: Compressor operating mode at high refrigerant temperatures and pressures.

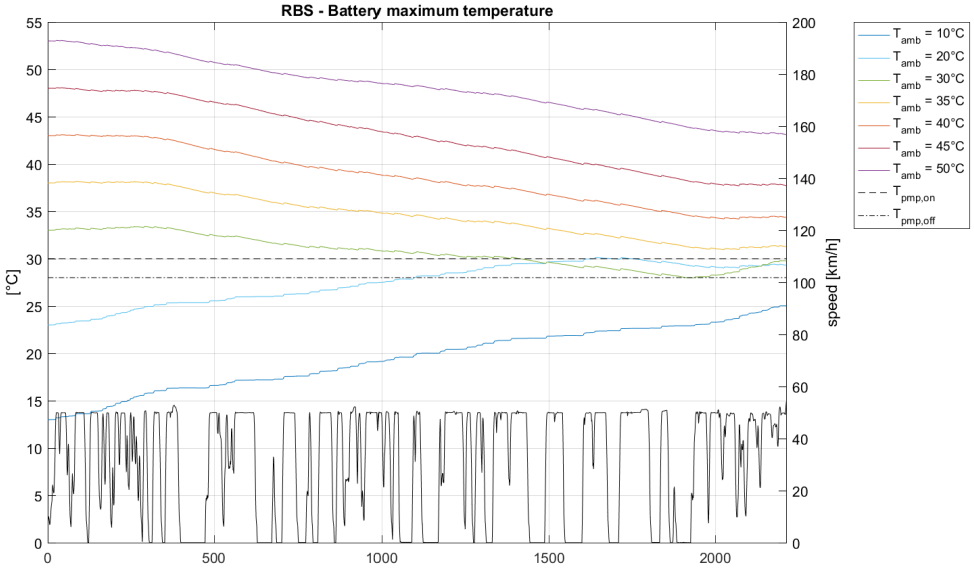

(a) Rule-Based Strategy.

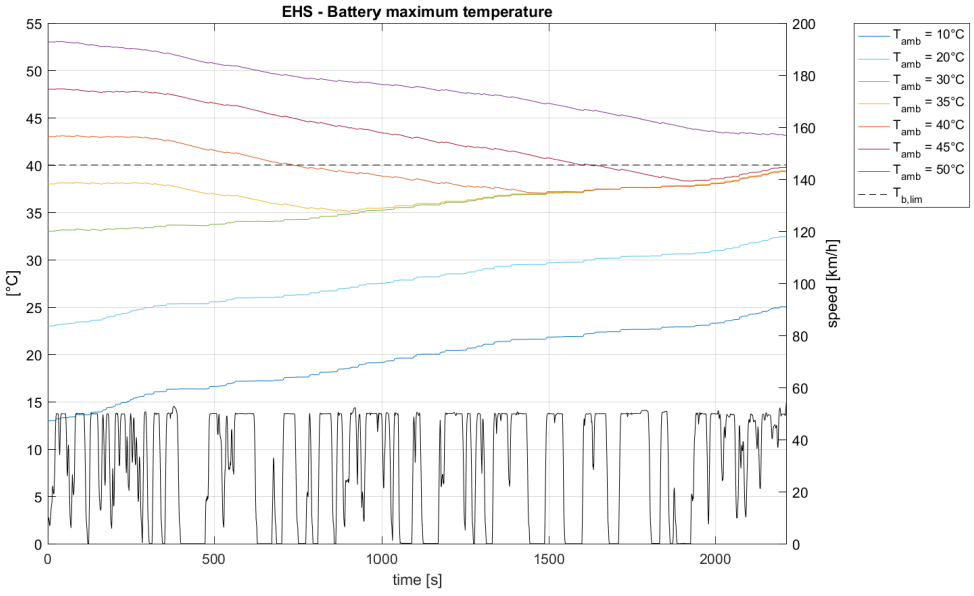

(b) eHorizon Strategy.

Figure 5.2: Test Case 1 – Behaviour of battery maximum temperature.

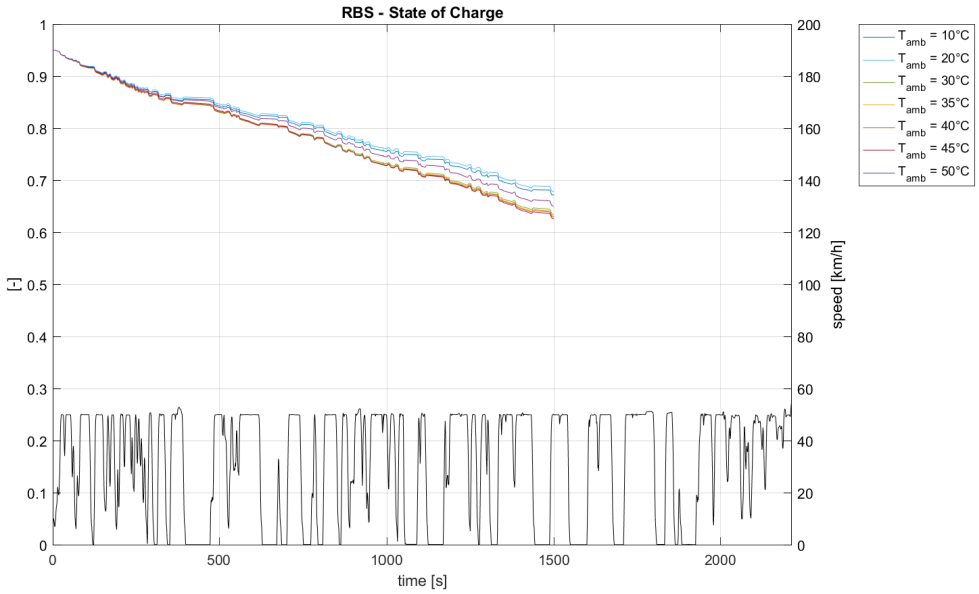

(a) Rule-Based Strategy.

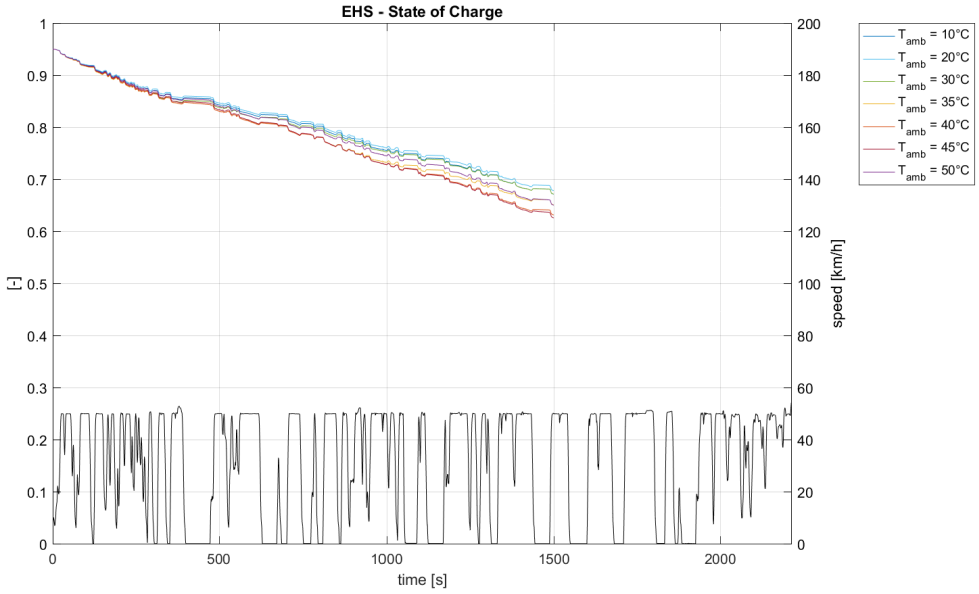

(b) eHorizon Strategy.

Figure 5.3: Test Case 1 – Behaviour of battery state of charge.

5.3 Test case 2 – Full RDE cycle

The entire RDE cycle is performed, and the eHorizon strategy is applied from the beginning of the cycle, i.e. at city enter, until the lower limit value of the SoC allowable in charge-depleting mode is reached. When this occurs, the RBS is switched on and remains active for the rest of the cycle. The control actuated by this strategy on battery cooling circuit is clear considering the behaviour of the battery maximum temperature (Fig. 5.6) after the beginning of the charge-sustaining mode, marked with a small dot. In this case, it can be seen that the temperature of the battery starts to decrease in consequence of the activation of the pump and the compressor because of the battery temperature upper threshold set for the heuristic strategy is exceeded for every test condition.

The behaviour of the battery state of charge is shown in Fig. 5.7, as well. The results obtained for the AER and the FC in each simulation are listed in Tab. 5.3 and Tab. 5.4, respectively.

Table 5.3: Test Case 2 – Results for the all-electric range.

T_{amb} [°C]	ξ_0 [%]	AER^{RBS} [%]	AER^{eHS} [%]
10	95	95.1	96.7
20	95	90.9	100.0
30	95	84.8	91.1
35	95	70.8	89.0
40	95	70.1	85.2
45	95	69.5	70.2
50	95	84.7	84.7

Concerning the all-electric range, it is clear that the behaviour of the SoC and the one of the AER are strictly correlated because of the later charge-sustaining mode starts, the longer is the trip performed in pure electric. In other words, as analogously seen in the previous test case, the all-electric range decreases with increasing environmental temperature, except for extreme ambient conditions. A sharp reduction of the AER can be noticed, as well, at middle high-temperatures for both the strategies. This fact is due to the relevant road gradient section which mainly characterizes the rural trip of the Bologna RDE cycle. The influence of road slope

Table 5.4: Test Case 2 – Results for the fuel consumption.

T_{amb} [°C]	ξ_0 [%]	FC^{RBS} [%]	FC^{eHS} [%]
10	95	89.2	88.9
20	95	91.5	88.0
30	95	96.8	93.6
35	95	100.0	95.2
40	95	99.2	97.5
45	95	99.6	99.6
50	95	96.5	96.5

on the state of charge in this part of the cycle is depicted in Fig. 5.4. It can be seen that by applying the RBS, at $T_{amb} = 35$℃ the energy consumption related to battery cooling makes the state of charge not high enough to overcome an up-hill section of the cycle, which is immediately followed by a down-hill one. Indeed, the benefit of energy recovering due to regenerative breaking in negative gradient roads is shown by the SoC behaviour at $T_{amb} = 30$℃. In the same way, this happens applying the eHorizon strategy, too, but the unfavourable slope-related condition occurs at higher ambient temperatures ($T_{amb} = 45$℃) due to the energy-efficient thermal management control operated by the predictive function during electric driving.

Furthermore, in order to neglect the effects of road gradient on the state of charge and the all-electric range, an additional test case with a null slope profile was needed to further investigate the parameters behaviour as a function of environmental temperature.

With regard to the fuel consumption, it is expected to present a reverse trend with respect to the behaviour of the all-electric range. That is why it is $FC^{eHS}(20℃) < FC^{eHS}(10℃)$ and $FC^{eHS}(50℃) < FC^{eHS}(45℃)$. Moreover, the highest value for FC obtained at $T_{amb} = 35$℃ with RBS active can be considered as an exception. As depicted in Fig. 5.5, the torque split control applied by the HCU is not the same in each simulation because of several parameters are taken into account at each calculation task. The instantaneous values of state of charge, wheels requested torque and vehicle speed have a great impact on the torque split factor evaluation [22].

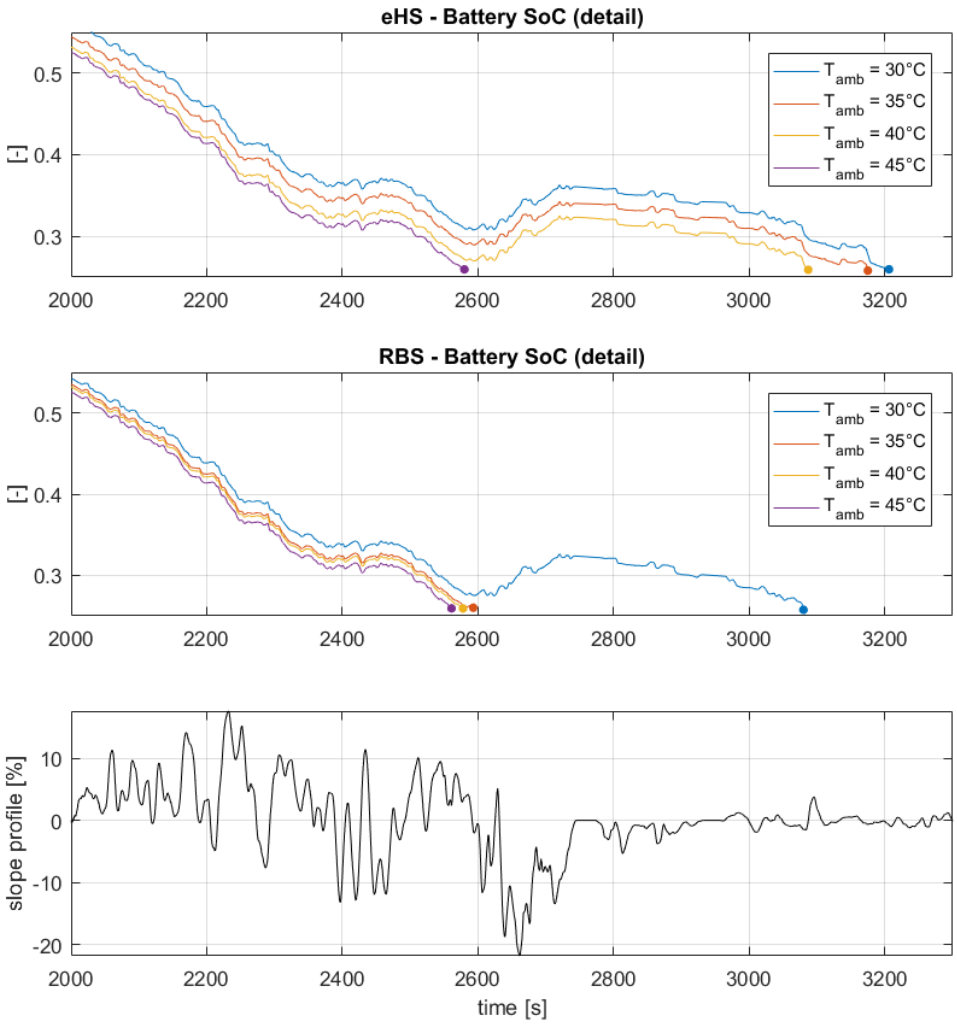

Figure 5.4: Test Case 2 – Effects of road slope on the state of charge.

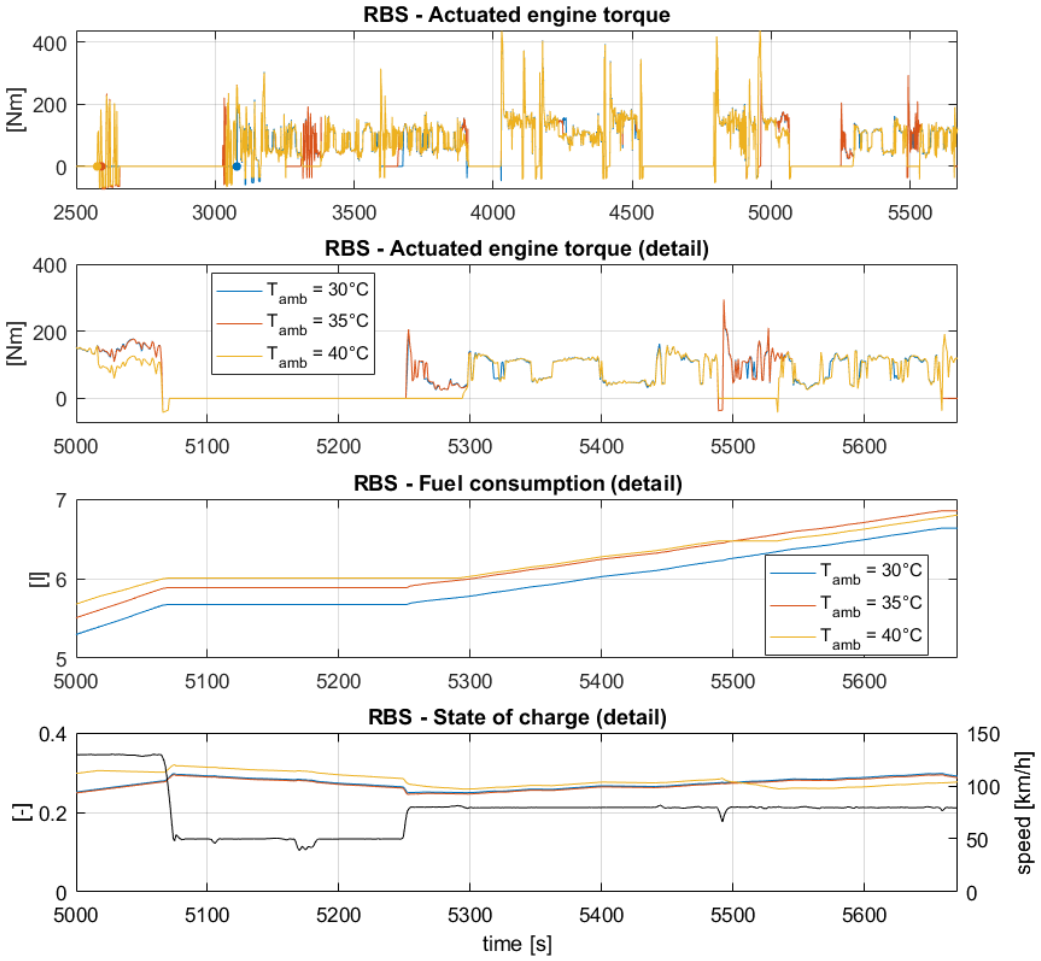

Figure 5.5: Test Case 2 – Analysis of fuel consumption.

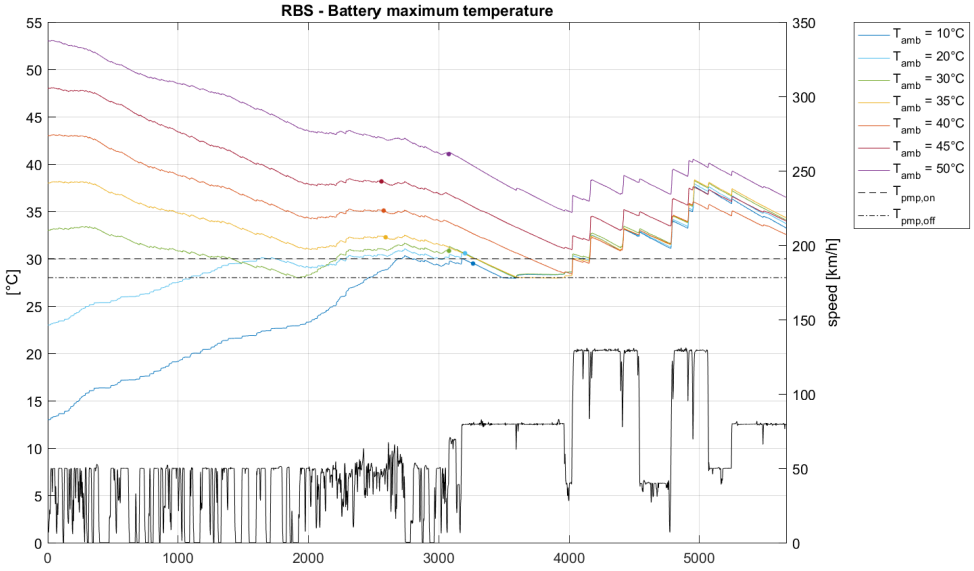

(a) Rule-Based Strategy.

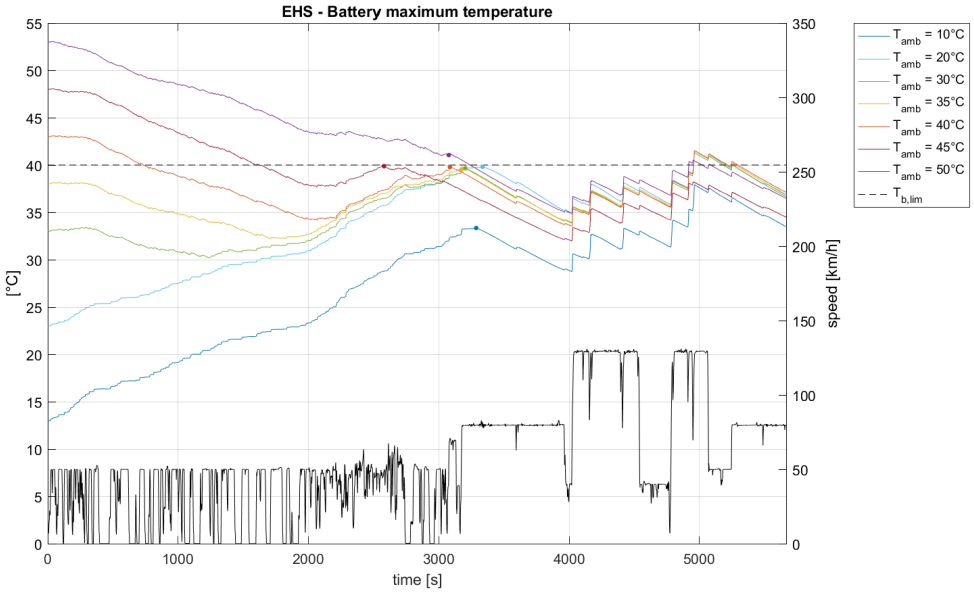

(b) eHorizon Strategy.

Figure 5.6: Test Case 2 – Behaviour of battery maximum temperature.

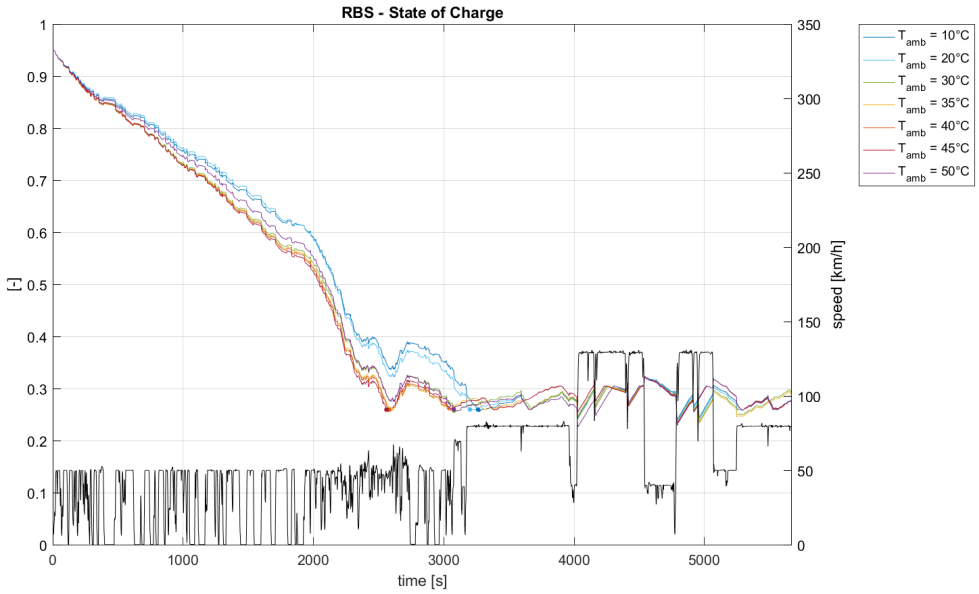

(a) Rule-Based Strategy.

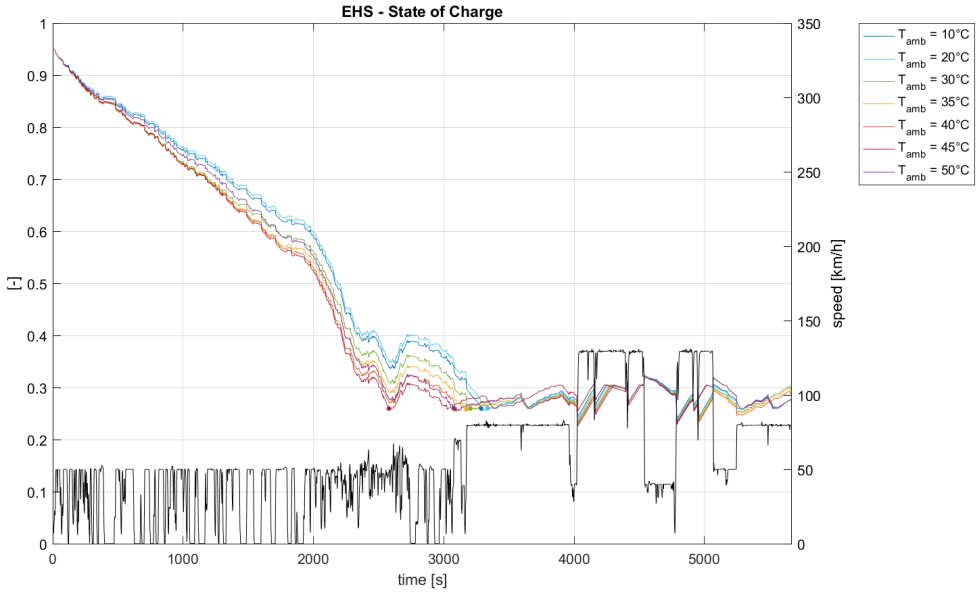

(b) eHorizon Strategy.

Figure 5.7: Test Case 2 – Behaviour of battery state of charge.

5.4 Test case 3 – Full RDE cycle with null slope

The behaviour of the maximum temperature and the SoC of the battery are shown in Fig. 5.9 and Fig. 5.10, respectively.

As expected, the values of the all-electric range (Tab. 5.5) and the fuel consumption (Tab. 5.6) vary directly in response to the changes of the ambient temperature, with the already known exceptions occurring at extreme environmental conditions.

Table 5.5: Test Case 3 – Results for the all-electric range.

T_{amb} [°C]	ξ_0 [%]	AER^{RBS} [%]	AER^{eHS} [%]
10	95	97.1	97.9
20	95	93.7	100.0
30	95	85.6	94.7
35	95	81.7	91.1
40	95	80.8	87.7
45	95	80.2	82.9
50	95	83.3	83.6

Table 5.6: Test Case 3 – Results for the fuel consumption.

T_{amb} [°C]	ξ_0 [%]	FC^{RBS} [%]	FC^{eHS} [%]
10	95	88.8	88.7
20	95	90.3	88.8
30	95	96.0	91.2
35	95	98.1	94.3
40	95	98.3	96.5
45	95	100.0	98.3
50	95	98.6	98.5

Moreover, even in this test case a relatively high value of the FC can be observed at high temperatures ($T_{amb} = 45$℃). As shown in Fig. 5.8, the major consumption of fuel at that ambient temperature is due to engine On at an unfavourable instant, in which the vehicle is facing a relevant acceleration phase. Consequently, in this case the engine applied torque is higher than the compared ones, and as a results

the fuel consumption strongly increases at engine ignition, especially because of cold start.

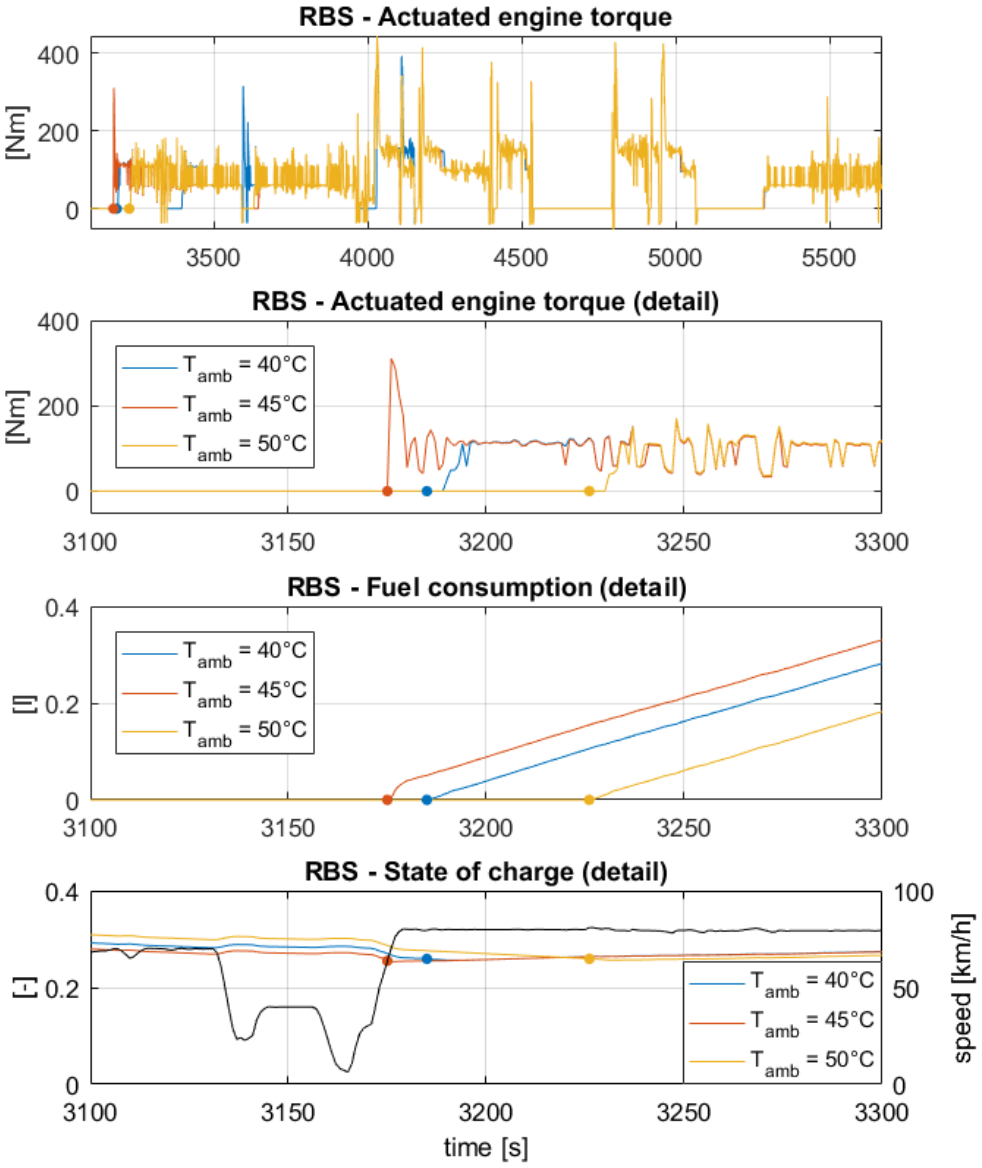

Figure 5.8: Test Case 3 – Analysis of fuel consumption.

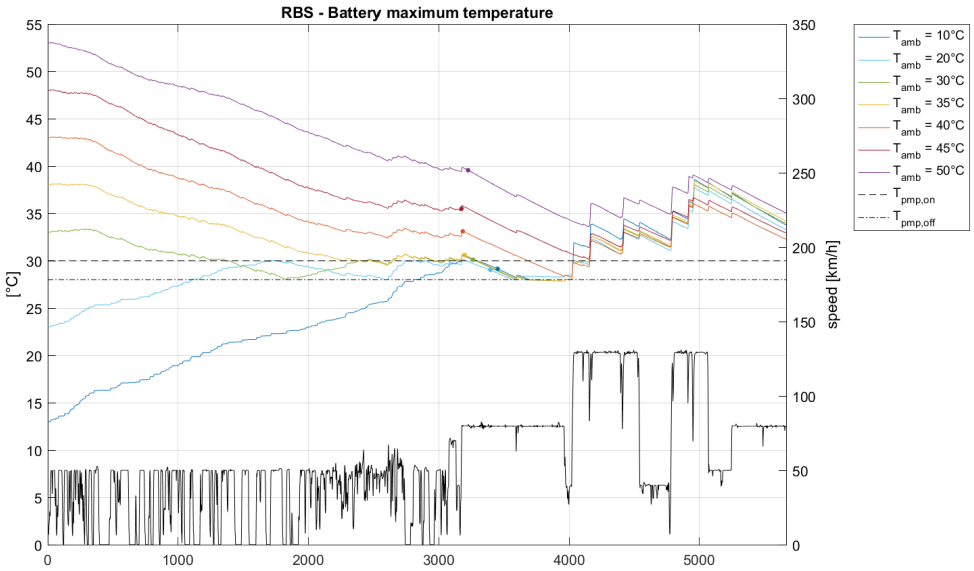

(a) Rule-Based Strategy.

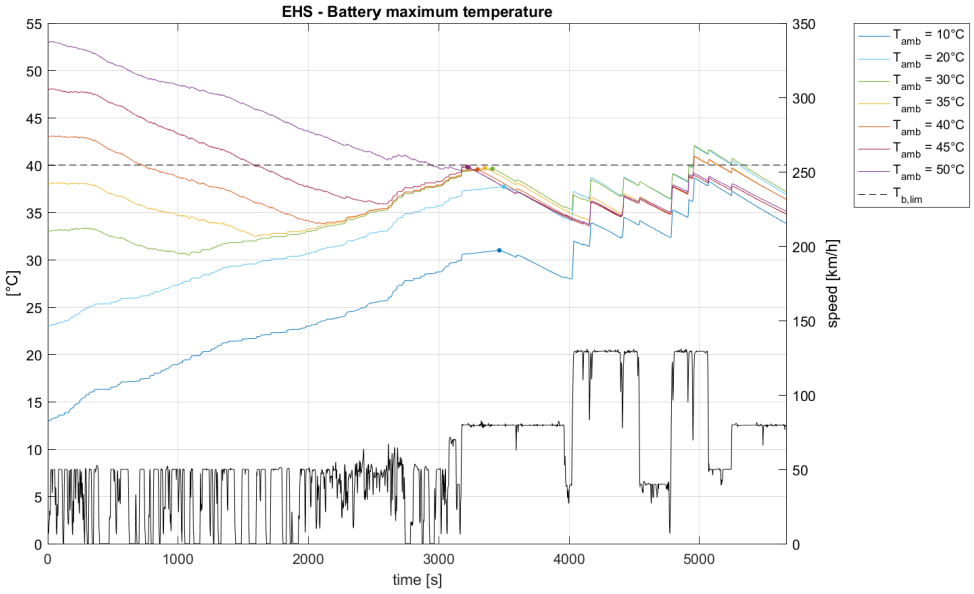

(b) eHorizon Strategy.

Figure 5.9: Test Case 3 – Behaviour of battery maximum temperature.

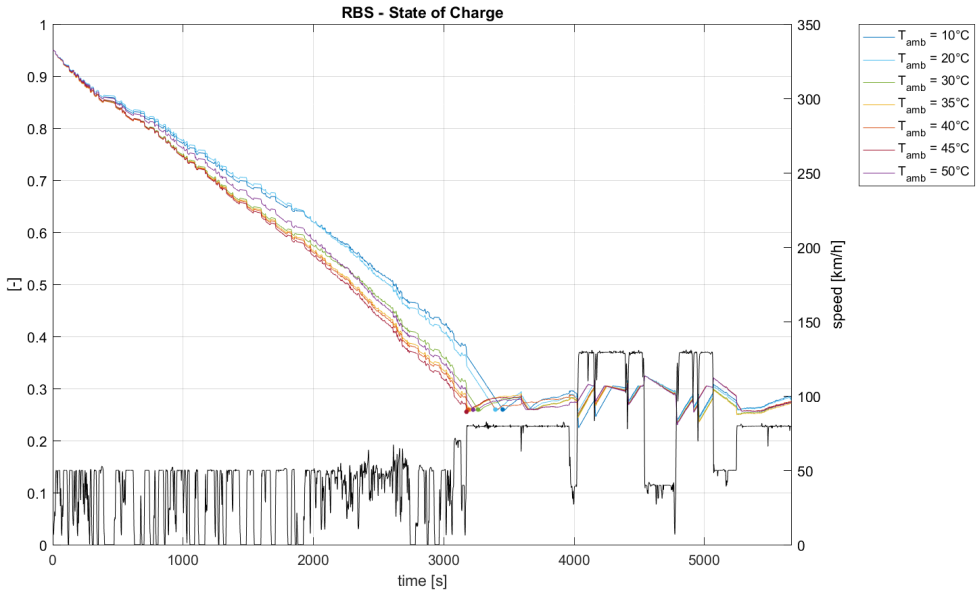

(a) Rule-Based Strategy.

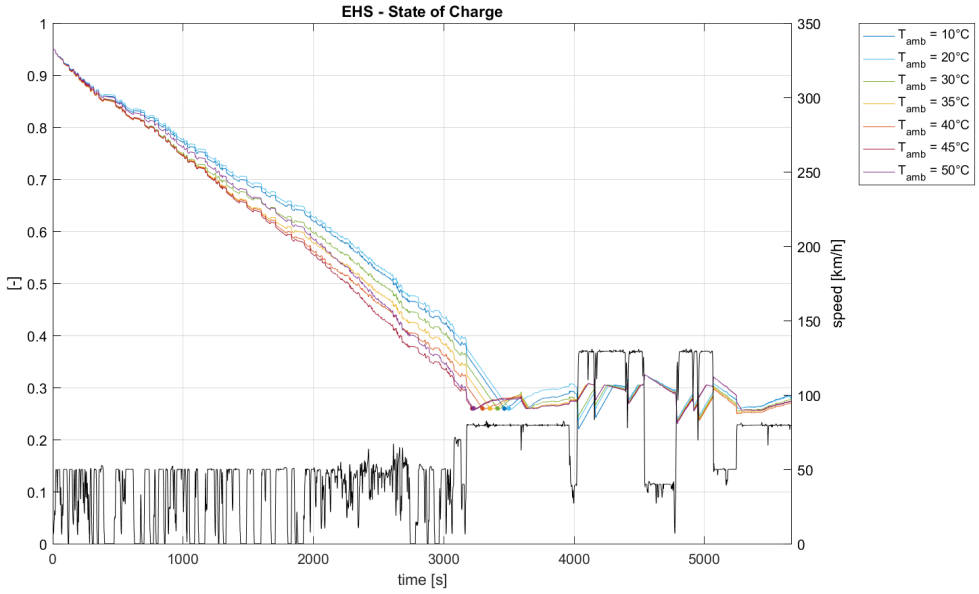

(b) eHorizon Strategy.

Figure 5.10: Test Case 3 – Behaviour of battery state of charge.

5.5 Conclusions

In order to compare the results over the all performed test cases, the maximum advantages obtained by applying the thermal management-oriented eHorizon strategy are summarized in Tab. 5.7.

Table 5.7: Maximum advantages of the eHorizon strategy compared to the Rule-Based one.

Test cases	$\max \Delta \xi_{c,out}$ [%]	$\max \Delta AER$ [%]	$\max \Delta FC$ [%]
1) city passage	+12.2% (30°C)	—	—
2) full RDE cycle	—	+25.80% (35°C)	4.80% (35°C)
3) full RDE cycle with null slope	—	+11.59% (35°C)	4.93% (30°C)

Finally, the following conclusions can be drawn

1. maximum performances of the eHS are obtained at middle-low ambient temperatures for the examined driving schedule. In particular, results have shown that for environmental temperatures up to $T_{\text{amb}} = 30$°C the predictive strategy allows to maintain the value of the SoC at city exit quite unchanged. This is due to the benefit related to the decreasing battery internal resistance at increasing environmental temperature, which makes the battery to deliver a lower electrical power due to lower power losses. It therefore follows that remarkable benefits in terms of AER extension can be achieved in cold scenarios and in the major part of summer ones;

2. maximum advantages of the eHS compared to the RBS take place at middle-high ambient temperatures, under which power from the battery is demanded by the heuristic strategy in order to cool down the component until its temperature drops below the lower threshold temperature related to pump activity;

3. same performances and then null advantages occur at extreme ambient temperatures, mainly because of battery cooling is never or always demanded at very low and high environmental conditions, respectively;

4. performances of both the strategies are influenced by the executed driving cycle. It has been proven that the road gradient has a strong impact on the state of charge, and consequently on the all-electric range.

Chapter 6

Conclusion and future jobs

The present activity is focused on the development development of a predictive thermal management function for plug-in hybrid electric vehicles. For this purpose, the cooling circuits of the vehicle have been physically and analytically modelled. Nevertheless, additional experimental data should be provided in order to accurately validate the battery cooling circuit and cabin model. However, the accuracy of temperature evaluation from the relative model has not compromised the present work.

Moreover, the results obtained and discussed in the previous chapter have highlighted the possibility of overcoming the energy economy challenge in PHEVs by means of a thermal management control strategy based upon navigation data. In particular, the knowledge of trip-related data has proved to be an essential to make the thermal control strategy to act in advance in a energy-efficient way.

Definitely, it can be said that the main goal of the present work has been achieved. Nevertheless, the developed eHorizon strategy can be considered an interesting starting point for further improving based on the following remarks

- enhance battery thermal dynamics modelling, maybe using a higher number of thermal masses,

- perform cabin model validation and calibration in order to analyse HVAC system impact on vehicle total energy consumption,

- a HVAC system control function oriented to energy saving and fuel consumption minimization might be developed, taking into account vehicle energy management (engine power request),
- improve the predictive thermal management control function by taking into account the overall vehicle driveline. This means that engine torque request and thus torque split factor are being evaluated, as well. The advantages of this further enhancing of the control function is related to the possibility of applying the eHorizon strategy not only in electric drive mode,
- improve the eHorizon strategy with a driver model in order to actually reconstruct the speed profile of the vehicle of a given trip. Additional navigation data can be used to achieve this objective on the base of ADASIS Protocol guidelines, maybe taking into account traffic events, upcoming stop and much more,
- extend the application of the eHorizon strategy to the middle and high temperature cooling subsystems,
- perform a simulations set using a different drive cycle in order to confirm the advantages reached by applying the eHorizon strategy,
- understand if implementing a slope event in the predictive thermal management control function could help to minimize energy consumption.

Appendix A

Tables

RDE Cycle

Fig. A.1: RDE cycle located in Bologna.

AMESim models layouts

- Fig. A.2: High-voltage battery cooling circuit model.
- Fig. A.3: Front-axle cooling circuit model.
- Fig. A.4: ISG cooling circuit model.
- Fig. A.5: Engine cooling circuit model.

AMESim models implementation in Simulink environment

Fig. A.6: Thermal management control-oriented models in MiL *Physical* block.

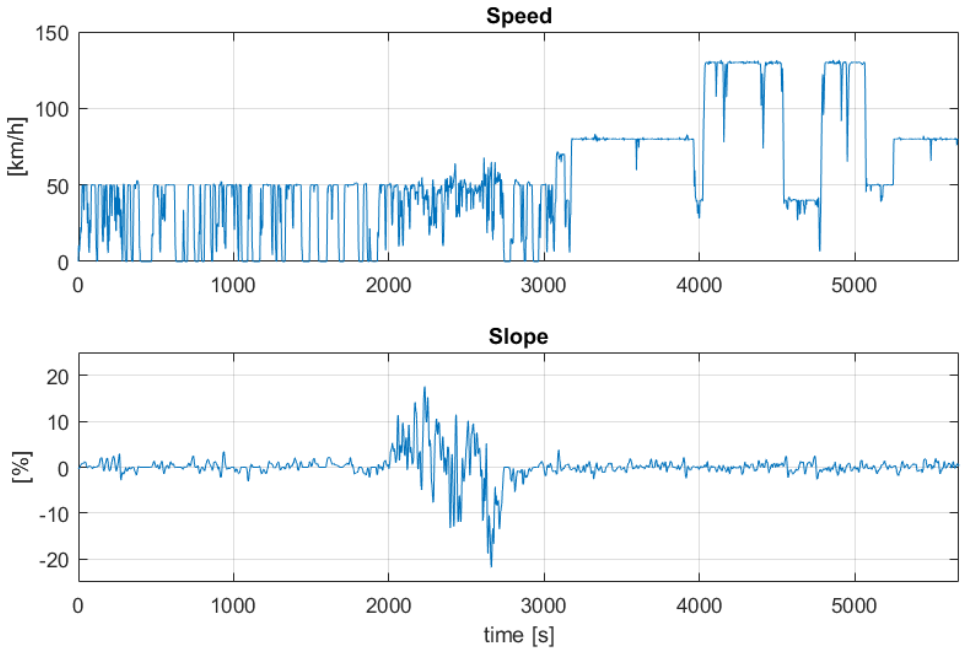

Figure A.1: RDE cycle located in Bologna.

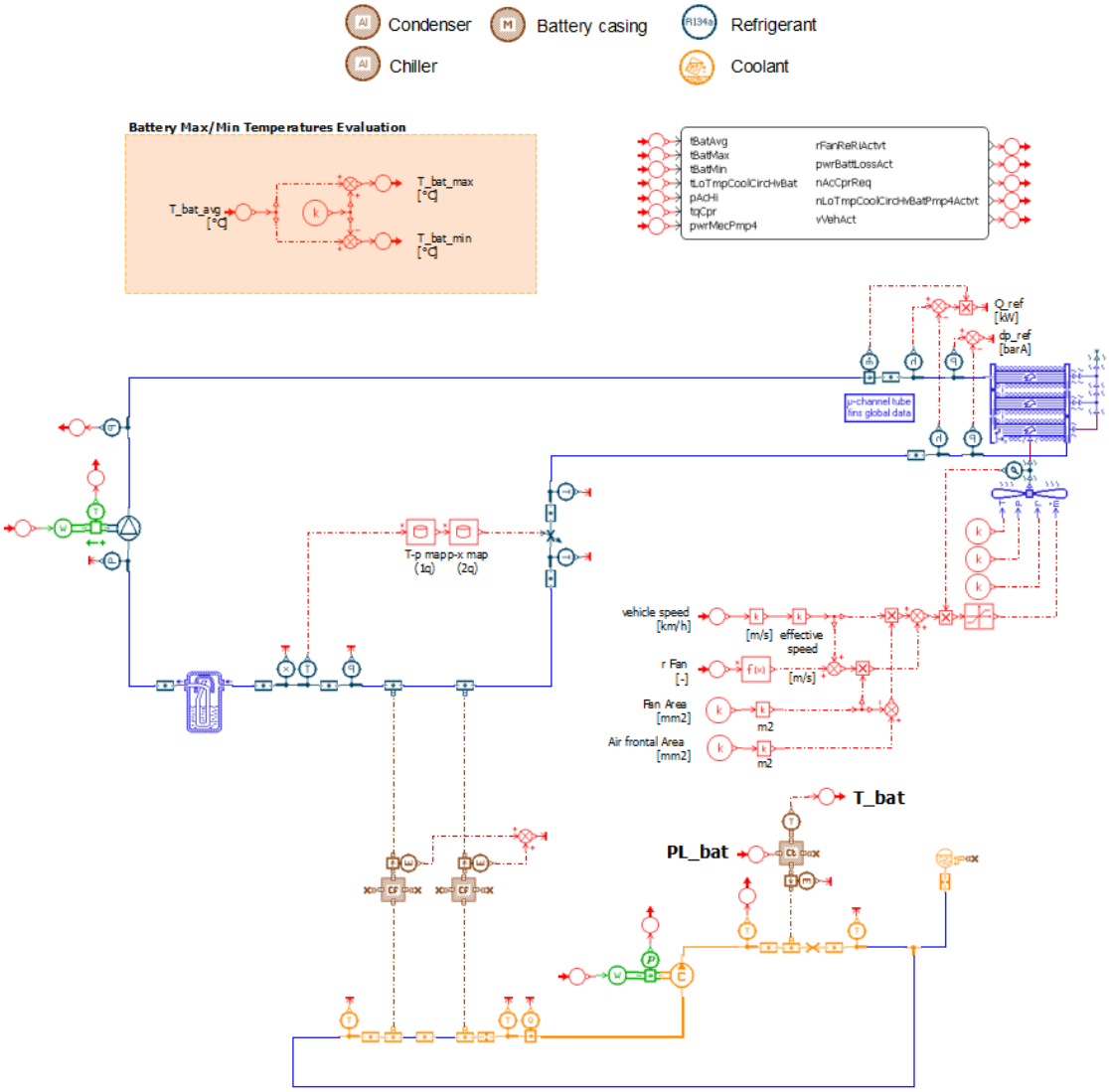

Figure A.2: High-voltage battery cooling circuit model.

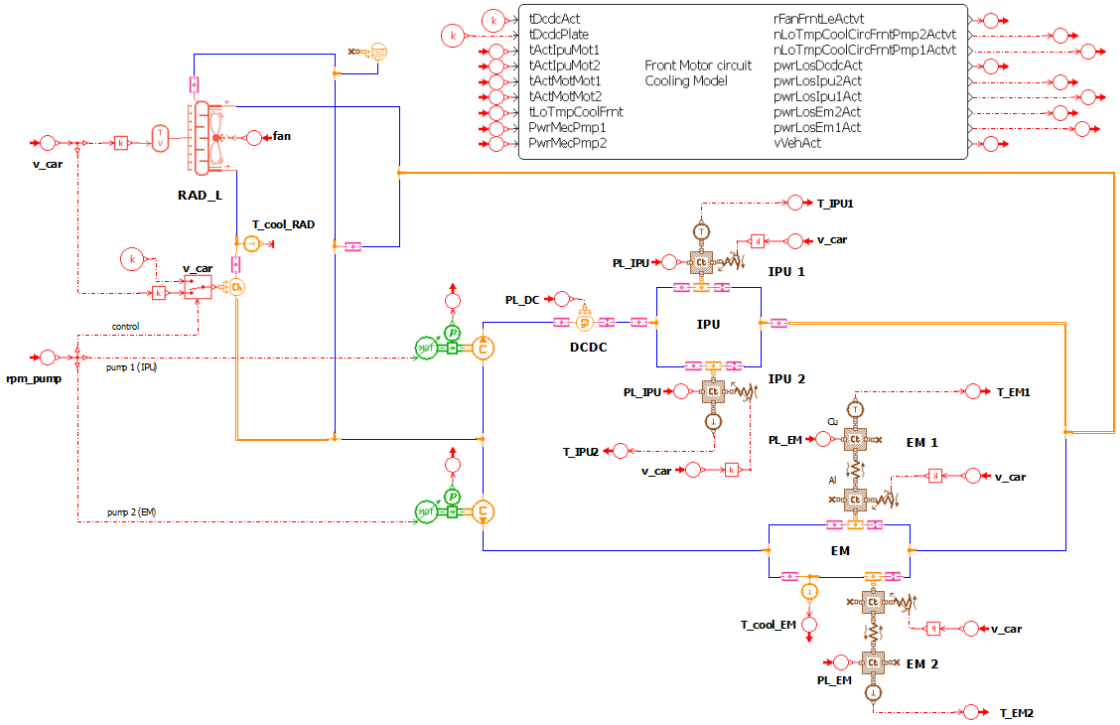

Figure A.3: Front-axle cooling circuit model.

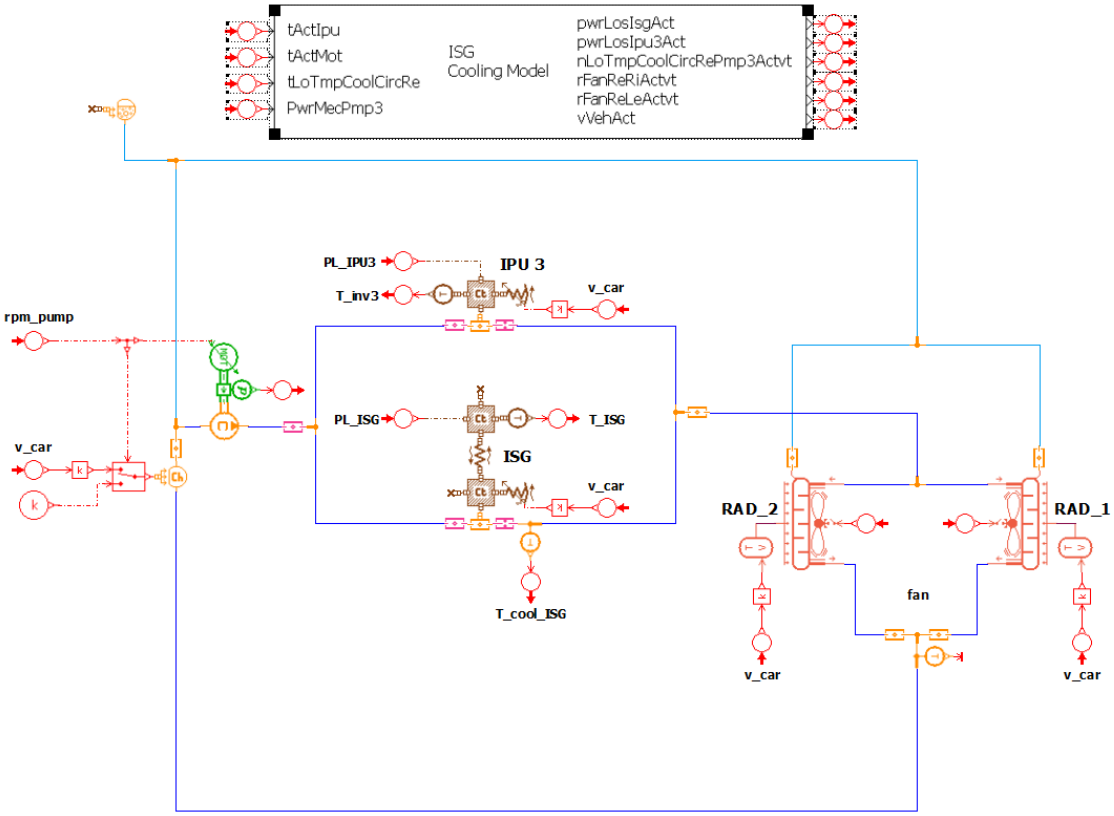

Figure A.4: ISG cooling circuit model.

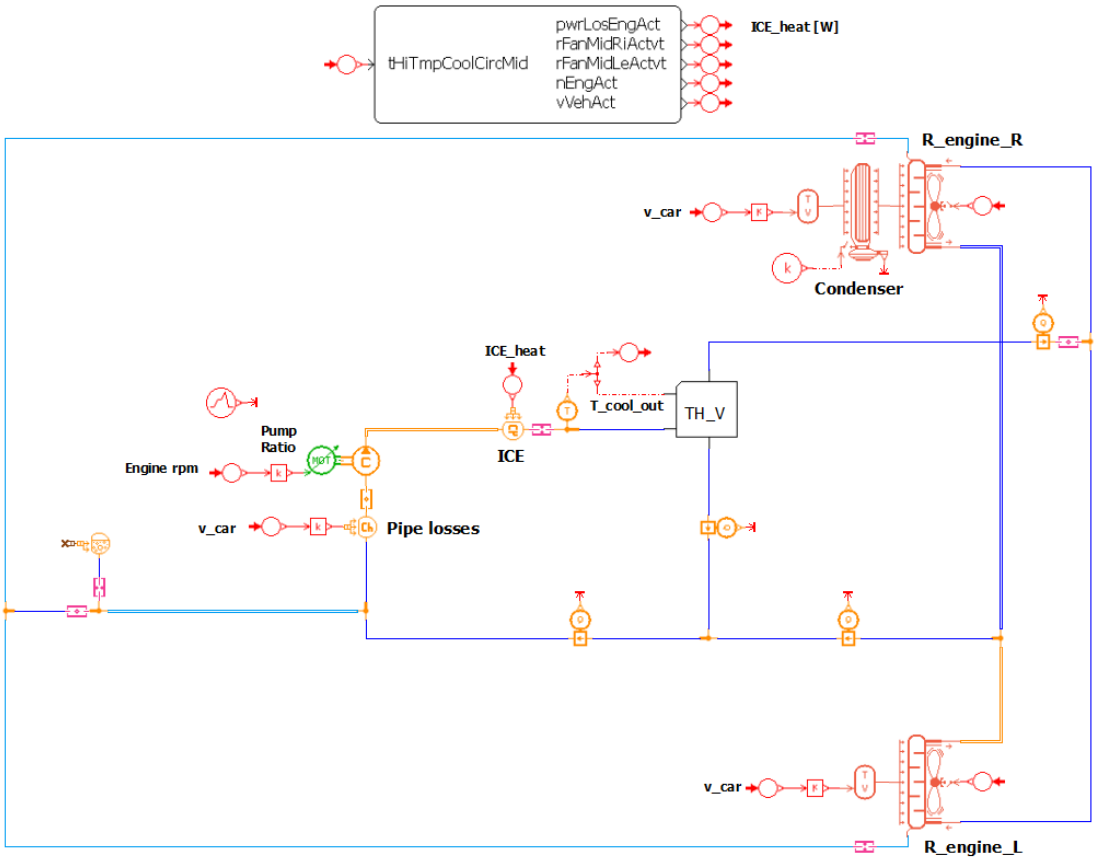

Figure A.5: Engine cooling circuit model.

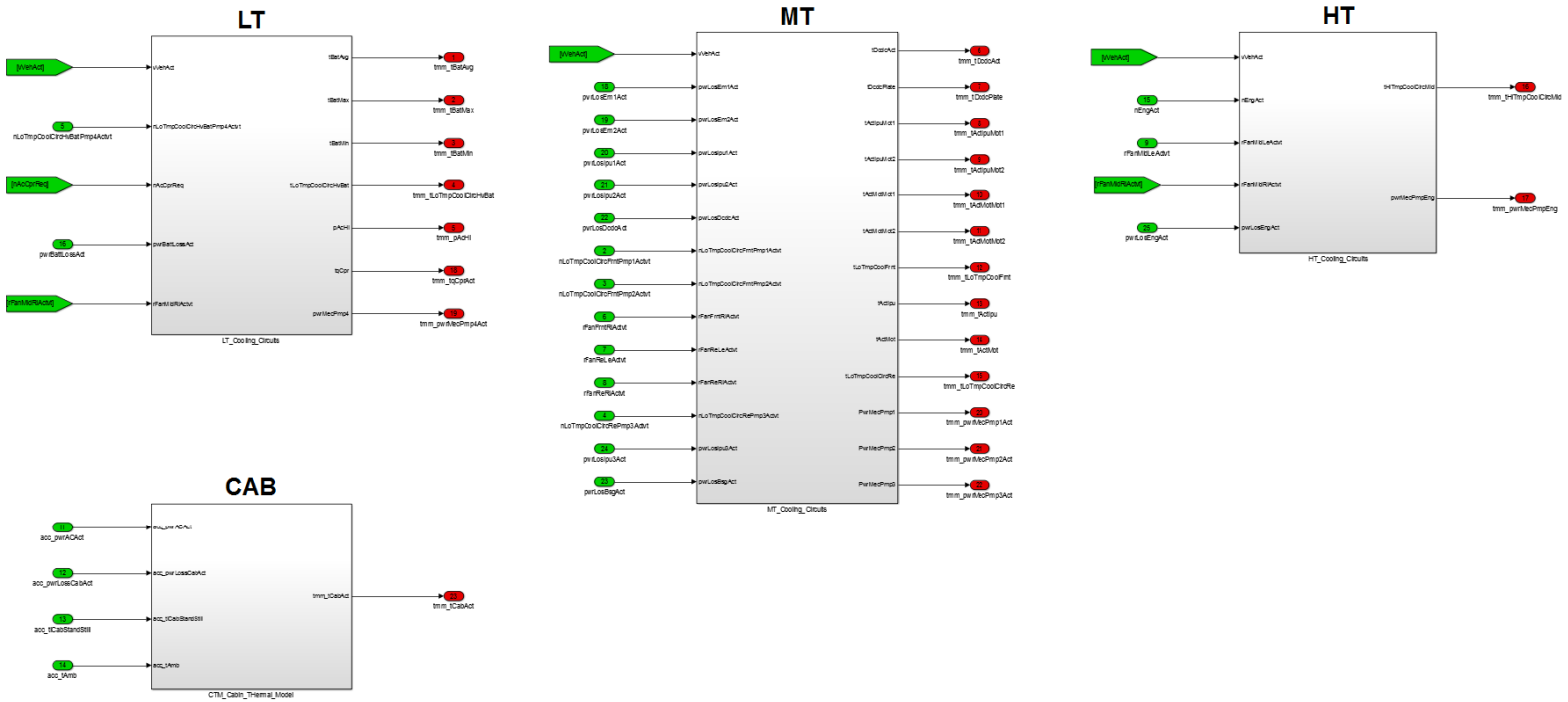

Figure A.6: Thermal management control-oriented models in MiL *Physical* block.

Bibliography

[1] "Real-Driving Emissions test procedure for exhaust gas pollutant emissions of cars and light commercial vehicles in Europe". International Council On Clean Transportation. **2017**. URL: https://goo.gl/GSgHTC.

[2] *Taxonomy and Definitions for Terms Related to Driving Automation Systems for On-Road Motor Vehicles*. SAE International, **2016**. DOI: 10.4271/J3016_201609.

[3] C. Ress, D. Balzer, A. Bracht, S. Durekovic, and Lowenau; J. "ADASIS Protocol for advanced in-vehicle applications" (). **2008**.

[4] R. Musat and E. Helerea. "Characteristics of the PTC Heater Used in Automotive HVAC Systems". Doctoral Conference on Computing, Electrical and Industrial Systems, 461–480. **2010**.

[5] K. Y. Kim, S. C. Kim, and M. S. Kim. "Experimental studies on the heating performance of the PTC heater and heat pump combined system in fuel cells and electric vehicles". *International Journal of Automotive Technology* 13.6 (**2012**), 971–977. DOI: 10.1007/s122390120099z.

[6] I. Dincer, H. S. Hamut, and N. Javani. *Thermal Management of Electric Vehicle Battery Systems*. 1st ed. Automotive Series. John Wiley & Sons, Inc., **2017**. ISBN: 978-1-118-90024-6.

[7] D. Neumeister, A. Wiebelt, and T. Heckenberger. "Systemeinbindung einer Lithium-Ionen-Batterie in Hybrid- und Elektroautos". *ATZ - Automobiltechnische Zeitschrift* 112.4 (**2010**), 250–255. DOI: 10.1007/BF03222156.

[8] L. Lefebvre. "Smart Battery Thermal Management for PHEV Efficiency". *OSGT Journal–Rev. IFP Energies nouvelles* 68.1 (**2013**), 149–164. DOI: 10.2516/ogst/2012076.

[9] M. R. Khan, M. J. Swierczynski, and S. K. Kær. "Towards an Ultimate Battery Thermal Management System: A Review". *Batteries* 3.9 (**2017**). DOI: 10.3390/batteries3010009.

[10] E. F. Camacho and C. Bordons. *Model Predictive Control*. 3rd ed. Springer International Publishing, **2007**. ISBN: 978-1-85233-694-3.

[11] H. Zomorodi, D. Yoon, and B. Ayalew. "Use of Predictive Information for Battery Pack Thermal Management" (**2017**), 5020–5025. DOI: 978-1-5090-5992-8/$31.00.

[12] H. Esen, T. Tashiro, D. Bernardini, and A. Bemporad. "Cabin heat thermal management in hybrid vehicles using model predictive control". 22nd Mediterranean Conference on Control and Automation. IEEE, **2014**. DOI: 10.1109/MED.2014.6961325.

[13] L. Morini. "Thermal management model for a Plug-In Hybrid Electric Vehicle". Master's Thesis. University of Bologna, **2017**. URI: http://amslaurea.unibo.it/id/eprint/12960.

[14] LMS AMESim Help guide.

[15] H. H. Al-Kayiem, M. F. B. M. Sidik, and Y. R.A.L Munusammy. "Study on the Thermal Accumulation and Distribution Inside a Parked Car Cabin". *American Journal of Applied Sciences* 7 (6), 784–789. ISSN: 1546-9239. **2010**.

[16] F. Brèque and M. Nemer. "Cabin Thermal Needs: Modeling and Assumption Analysis". *Proceedings of the 12th International Modelica Conference, Prague, Czech Republic, May 15-17, 2017*. 132. Linköping University Electronic Press, **2017**, 771–781. DOI: 10.3384/ecp17132771.

[17] D. Marcos, F. J. Pino, C. Bordons, and J. J. Guerra. "The development and validation of a thermal model for the cabin of a vehicle". *World Electric Vehicle Journal* 5.1 (**2014**), 646–656. DOI: 10.1016/j.applthermaleng.2014.02.054.

[18] A. Lajunen. "Energy Efficiency and Performance of Cabin Thermal Management in Electric Vehicles". WCX™17: SAE World Congress Experience. SAE International, **2017**. DOI: 10.4271/2017-01-0191.

[19] S. Gmeiner, P. Rajan, J. Gissing, and D. Backes. "VOSS Innovative Valve Technology for Thermal Management". 25th Aachen Colloquium Automobile and Engine Technology. **2016**, 471–490.

[20] T. J. Böhme and B. Frank. *Hybrid Systems, Optimal Control and Hybrid Vehicles. Theory, Methods and Applications*. 1st ed. Advances in Industrial Control Series. Springer International Publishing, **2017**. ISBN: 978-3-319-51315-7.

[21] *BS ISO 10521-1:2006. Road vehicles. Road load. - Part 1: Determination under reference atmospheric conditions*. English. **2006**. DOI: 10.3403/30101315U.

[22] L. Guzzella and A. Sciarretta. *Vehicle Propulsion Systems. Introduction to Modeling and Optimization*. 3rd ed. Springer International Publishing, **2013**. ISBN: 978-3-642-35912-5.